RESEARCH ARTICLE

Basin Research |AS EAGE WILEY

Neogene aridification and lake development in the Issyk-Kul basin, Kyrgyzstan

Anna Kudriavtseva[1,2] | Edward R. Sobel[1] | Alexandru T. Codilean[2,3] |
Maud J. M. Meijers[4,5] | Andreas Mulch[5,6] | Gregory D. Hoke[7] | David Fink[8] |
Alexander V. Mikolaichuk[9] | Réka-H. Fülöp[2,8] | Klaus M. Wilcken[8] |
T. Gabriel Enge[10]

[1]Institute of Geosciences, University of Potsdam, Potsdam-Golm, Germany

[2]School of Earth, Atmospheric and Life Sciences, University of Wollongong, Wollongong, New South Wales, Australia

[3]ARC Centre of Excellence for Australian Biodiversity and Heritage (CABAH), University of Wollongong, Wollongong, New South Wales, Australia

[4]Institute of Earth Sciences, NAWI Graz Geocenter, Universität Graz, Graz, Austria

[5]Senckenberg Biodiversity and Climate Research Centre, Frankfurt am Main, Germany

[6]Institute of Geosciences, Goethe University Frankfurt, Frankfurt am Main, Germany

[7]Department of Earth and Environmental Sciences, Syracuse University, Syracuse, New York, USA

[8]Australian Nuclear Science and Technology Organisation (ANSTO), Lucas Heights, New South Wales, Australia

[9]Institute of Geology, National Academy of Sciences, Bishkek, Kyrgyzstan

[10]Research School of Earth Sciences, The Australian National University, Canberra, Australian Capital Territory, Australia

Correspondence
Anna Kudriavtseva, Institute of Geosciences, University of Potsdam, Potsdam-Golm 14476, Germany.
Email: kudriavtseva.anna.a@gmail.com

Abstract

Uplift of the Tian Shan range modified regional climate during Cenozoic aridification in Central Asia. This study presents facies analyses and Neogene oxygen and carbon isotopic records from magnetostratigraphically dated terrestrial sedimentary sections on the southern side of the intermontane Issyk-Kul basin in the Kyrgyz Tian Shan and $^{26}Al/^{10}Be$ isochron burial ages from the southern and eastern sides of the basin. The $\delta^{18}O$ and $\delta^{13}C$ data show a positive ca. 2‰ shift in values between ca. 8 and 7 Ma and a change from a negative to a positive trend. This change is attributed to the upwind growth of the Kyrgyz, Kungey and Trans Ili (Zaili) ranges, which diverted the westerlies, thereby changing the Issyk-Kul basin from a windward to a leeward position, enhancing aridification and establishing the modern-day spring and summer precipitation regime within the basin. Two 4 to 5 Ma $^{26}Al/^{10}Be$ isochron burial ages constrain the onset of Sharpyl Dak deposition on the eastern side of the basin; southward paleocurrent directions there suggest the eastward growth of the Kungey range in the Pliocene. Increased subsidence on the southern side of the basin and local tectonically

induced river system reorganization led to the commencement of lake formation at ca. 5 Ma, followed by a ca. 2 Ma local depositional hiatus. The transition from sandstones of the Chu sedimentary group to conglomerates of the Sharpyl Dak group, marking a change from fluvial-alluvial deposits to a proximal alluvial fan, is dated at 2.6–2.8 Ma by ^{26}Al/^{10}Be isochron burial dating on the southern side of the basin, driven either by tectonics or Northern Hemisphere glaciation. This study concludes that the late Miocene–Pliocene northward growth of Tian Shan significantly altered environmental conditions within the range, preventing the moisture-bearing westerlies from reaching the intermontane Issyk-Kul basin and promoting lake formation and expansion.

KEYWORDS

Cenozoic aridification, Central Asia, cosmogenic ^{26}Al/^{10}Be, tectonic uplift, westerlies, δ^{18}O and δ^{13}C stable isotopes

1 | INTRODUCTION

Central Asia is the largest arid region in the Northern Hemisphere. Aridity there has increased during the Cenozoic (e.g. Caves et al., 2016; Fang et al., 2020; Li et al., 2018; Wasiljeff et al., 2022). A decrease in the moisture flux delivered by the northern midlatitude westerlies, which transport moisture eastward across Eurasia, likely played a major role in aridification (e.g. Caves et al., 2015). Decreased westerly moisture transport resulted from Cenozoic global cooling (e.g. Bosboom, Abels, et al., 2014; Miao et al., 2012) and Paratethys retreat (e.g. Bosboom, Dupont-Nivet, et al., 2014; Bosboom et al., 2017; Kaya et al., 2019; Ramstein et al., 1997), while surface uplift of the Tibetan Plateau, Tian Shan and other mountain ranges created topographic barriers to moisture input (e.g. Caves et al., 2014; Chang et al., 2021; Kent-Corson et al., 2009; Liu et al., 2014; Sun et al., 2015).

The Issyk-Kul intermontane basin in the Kyrgyz Central Tian Shan (Figure 1) contains a Neogene geological record that provides valuable information about the complex interactions between tectonic deformation and Central Asian climate at global and regional scales (e.g. Macaulay et al., 2016; Oberhänsli & Molnar, 2012). Nevertheless, details of how and why this internally drained basin formed remain unclear. Within the Tian Shan range, changes in the magnitude of precipitation and the vegetation system can reflect either globally or locally driven climatic changes or a combination of both. Local and regional climate and landscape can be modified by tectonic surface uplift, which influences the distribution of precipitation, river discharge and erosion rates, while global climatic changes alter overall moisture delivery to the region, vegetation and the characteristics of surface processes

Highlights

- Stable isotopes and CRN burial dating define changes in climate and tectonics in Issyk-Kul basin.
- Basin position changed from windward to leeward at 8–7 Ma due to northward growth of the Tian Shan.
- Changes in moisture supply established drying trend and modern-day precipitation regime.
- Tectonically induced river system reorganization led to lake formation at ca. 5 Ma.
- Change from fine-grained fluvial to coarse-grained alluvial deposits occurred diachronously in basin.

(e.g. Chamberlain et al., 2012; Dupont-Nivet et al., 2007; Herbert et al., 2016; Ramstein et al., 1997; Rowley & Garzione, 2007). The spatial and temporal distribution of paleoprecipitation proxy data, such as oxygen and carbon isotopes, has been used to distinguish between the influence of tectonic and global climatic factors (e.g. Caves Rugenstein & Chamberlain, 2018; Miao et al., 2012). Here, we investigate differences in timing of regional environmental change and corresponding global climate change to identify the impact of changing relief and elevation of the regional mountain belts.

Available paleoclimate records from northern Central Asia are relatively scarce compared with data from the Chinese portion of East Asia; moisture, delivered by the westerlies, was blocked from reaching the latter region as a result of the development of complex topography (e.g.
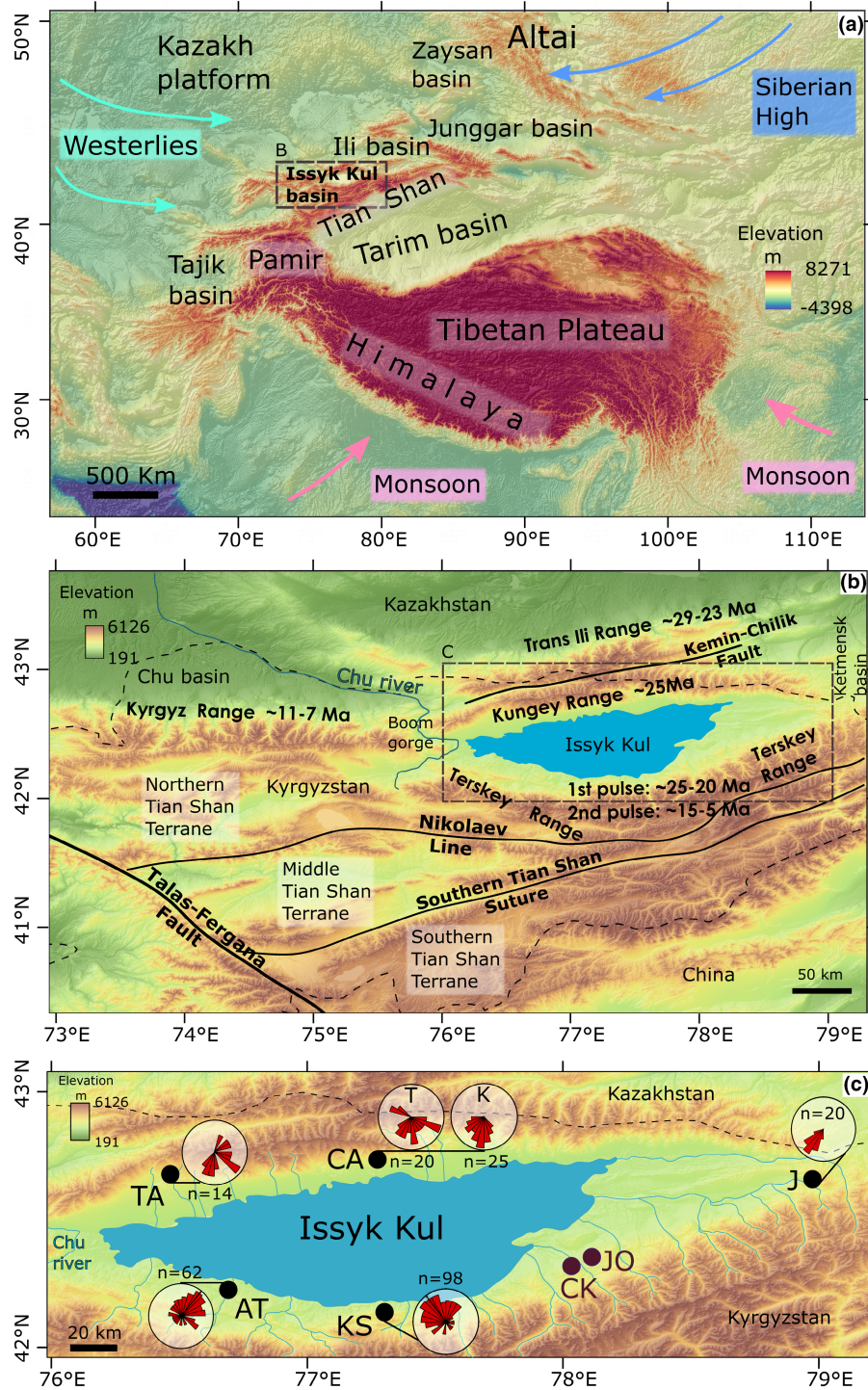
FIGURE 1 (a) Topographic map of Central Asia based on SRTM90 digital elevation data showing major ranges and sedimentary basins. Light blue arrows—westerly winds; dark blue arrows—Siberian High; pink arrows—monsoons. (b) Topographic map of the Kyrgyz Central Tian Shan showing the main faults, positions of the basement terranes, the north-flowing Chu river, country borders (dashed line), and the main ranges with estimated ages for the onset of Cenozoic deformation: Kyrgyz Range (Bullen et al., 2001, 2003; Sobel, Oskin, et al., 2006); Terskey Range (Macaulay et al., 2013, 2014, 2016); Kungey and Trans Ili Ranges (de Grave et al., 2013; De Pelsmaeker et al., 2015). (c) Topographic map of the study area and paleocurrent directions measured in imbricated clasts and cross-bedded sandstones. Localities of this study: AT—Ak Terek; KS—Kaji Say; J—Jergalan; TA—Toru Aygir; CA—Cholpon Ata. T—Terskey member of the Chu group, K—Kungey member of the Chu group. Localities from Wack et al. (2014) and Macaulay et al. (2016): CK—Chon Kyzylsu; JO—Jeti Oguz. Dashed line shows country borders.

Dettman et al., 2003; Fan et al., 2007; Graham et al., 2005; Hough et al., 2011; Kent-Corson et al., 2009; Li et al., 2016; Zhuang et al., 2011). The >2500-km-long Tian Shan (also called the Tien Shan, i.e. the Heavenly mountains in Chinese) presently forms a significant orographic barrier to the westerlies, which creates a distinctive difference in seasonality of precipitation on its windward and leeward sides, as well as within the range (e.g. Baldwin & Vecchi, 2016). Creation of an orographic barrier occurred during the late Oligocene by growth of the Pamir and western Tian Shan (Wang et al., 2020).

We present a study of the sedimentary record preserved in the Issyk-Kul basin, which is located to the west and/or north of other published Cenozoic climatic records from this region: Tajik basin, Ili basin, Junggar basin and Zaysan basin (Figure 1a; Caves et al., 2014, 2017; Charreau et al., 2012; Frisch, Voigt, Verestek, et al., 2019; Hellwig et al., 2018; Prud'homme et al., 2021; Wang et al., 2020). The Issyk-Kul basin is connected to the Ketmensk basin to the east and is situated between the Terskey, Kungey, Trans Ili (also called Zaili) and the Kyrgyz ranges; these ranges are all part of the northern Tian Shan (Figure 1b). The Issyk-Kul basin contains up to 4 km of Oligocene to Quaternary strata, which record the sedimentary response to regional climate change and proximal tectonic processes. The first magnetostratigraphic dating of the fossil-poor sedimentary deposits of the Chon Kyzylsu and Jeti Oguz sections in the southeastern part of the Issyk-Kul basin (Wack et al., 2014) shows early to middle Miocene ages of these deposits. Macaulay et al. (2016) presented the first oxygen (δ^{18}O) and carbon (δ^{13}C) stable isotope data for the dated sections. Roud et al. (2021) presented late Miocene to early Pleistocene magnetostratigraphic age models for two new sections (Kaji Say and Ak Terek) from the southern flank of the Issyk-Kul basin and revised age models for Wack et al.'s (2014) stratigraphically older sections.

Here, we present facies analyses from five stratigraphic sections around lake Issyk-Kul (Kaji Say, Ak Terek, Toru Aygir, Cholpon Ata and Jergalan; Figure 1c), ^{26}Al/^{10}Be isochron burial ages from three of them (Kaji Say, Ak Terek, Jergalan), and δ^{18}O and δ^{13}C records of pedogenic, fluvial and lacustrine carbonates from the two late Miocene–early Pleistocene sections (Kaji Say, Ak Terek) dated by Roud et al. (2021) using magnetostratigraphy. Our ^{26}Al/^{10}Be isochron burial ages refine the age model for these deposits and constrain when lake Issyk-Kul formed. We combine our data with published records from stratigraphically older nearby sections (Macaulay et al., 2016) to present nearly complete Miocene–Pliocene δ^{18}O and δ^{13}C records and to study how the growth of the adjacent mountain ranges influenced the environmental conditions in the Issyk-Kul basin. Comparing our

combined stable isotopic record from the Issyk-Kul basin with data from across the region provides new insights into the role of the Tian Shan and its interaction with the westerlies under a globally cooling climate in the late Neogene.

2 | GEOLOGICAL AND CLIMATIC SETTING

2.1 | Cenozoic reactivation of the Tian Shan

The Cenozoic India–Asia collision led to the creation of the Tibetan Plateau and the Pamir and tectonically reactivated the Tian Shan and Altai ranges to the north during the late Oligocene–Miocene (Figure 1a; e.g. Abdrakhmatov et al., 2002; Glorie & De Grave, 2016; Molnar & Tapponnier, 1975; Sobel, Chen, et al., 2006). The Tian Shan is a 2500-km-long orogenic belt with present-day shortening rates of up to 20 mm.yr^{-1} (Abdrakhmatov et al., 1996; Zubovich et al., 2010). The Central Kyrgyz Tian Shan and the Chinese Central and Western Tian Shan are bounded by the Tarim basin to the south and the Kazakh platform to the north. The Issyk-Kul basin is situated within the Northern terrane of the Central Kyrgyz Tian Shan (Figure 1b).

The Northern, Middle and Southern Tian Shan terranes comprise the three major fault-bounded Palaeozoic terranes of the Central Kyrgyz Tian Shan (Figure 1b; Bakirov & Maksumova, 2001; Biske & Seltmann, 2010). The Northern terrane is built of late Ordovician to early Silurian granites, along with Precambrian metamorphic rocks and early Palaeozoic ophiolites, overlain by Ordovician sedimentary rocks (Bakirov & Maksumova, 2001; Maksumova et al., 2001; Windley et al., 2007). The Middle Tian Shan comprises Paleoproterozoic metamorphic rocks, overlain by Neoproterozoic and Palaeozoic clastic and volcanic rocks, as well as middle Devonian to early Permian marine carbonate and clastic rocks (Bakirov & Maksumova, 2001; Biske, 1996; Maksumova et al., 2001; Seltmann et al., 2011). The Southern Tian Shan consists of Silurian–lower Permian ophiolites and sedimentary rocks of a Late Palaeozoic collisional system with early Permian granites (Biske, 1996; Maksumova et al., 2001; Seltmann et al., 2011).

Palaeozoic deformation of the Tian Shan started in the late Carboniferous and the late Permian–Triassic collision led to the development of the Southern Tian Shan Suture and large sinistral strike-slip faults, including the Nikolaev line, which separate the terranes (Figure 1b; e.g. Bazhenov et al., 1999; Bazhenov & Mikolaichuk, 2004). Afterwards, parts of the Tian Shan were reactivated during

the Mesozoic and early Cenozoic (see figure 8 in Macaulay et al., 2014 for a detailed depiction).

The most recent deformation started in the late Oligocene after a period of tectonic quiescence. Deformation during the Miocene led to the formation of a vast, east–west trending mountain range (e.g. De Grave et al., 2013; Macaulay et al., 2013). Thermochronological data show that the Terskey range on the south side of the Issyk-Kul basin and the Trans Ili range on the north side of the basin started deforming in the late Oligocene–early Miocene (De Grave et al., 2013; De Pelsmaeker et al., 2015; Macaulay et al., 2013, 2014, 2016). Deformation within the Terskey range propagated eastward and reached the eastern side of the Issyk-Kul basin by the middle Miocene (Macaulay et al., 2014). The onset of deformation in the Kungey range, separated from the Trans Ili range by the Kemin-Chilik fault, also started in late Oligocene, as defined by thermochronology (de Grave et al., 2013; De Pelsmaeker et al., 2015). However, paleocurrent data suggest that the sediments from the Terskey range were deposited on the southern flank of the Kungey range area until the late Miocene, with a late Miocene–early Pliocene estimated age of initiation of significant deformation there (Selander et al., 2012). Thermochronological data show that deformation of the Kyrgyz range, to the northwest of the Issyk-Kul basin, initiated in the present centre of the range during the late Miocene and propagated eastward (Bullen et al., 2001, 2003; Sobel, Oskin, et al., 2006).

2.2 | Precipitation in the Tian Shan

Today, the entire Tian Shan range forms a significant topographic barrier to westerly winds and is responsible for the differences in seasonality of precipitation with dominantly winter–spring precipitation on the windward (northwestern) side of the Tian Shan and summer precipitation within the range itself and on its leeward (southeastern) side (Baldwin & Vecchi, 2016). However, during the late Cretaceous, a low-relief and low-elevation erosion surface extended over much of the Tian Shan region; therefore, the orographic barrier post-dates this time (e.g. Bullen et al., 2001, 2003; Macaulay et al., 2014; Sobel, Oskin, et al., 2006; Yang et al., 2014). The moisture supply in Central Asia has been dominated by the westerlies since at least the Eocene (Bougeois et al., 2018; Caves et al., 2015; Licht et al., 2016). The Tian Shan and Pamir have interacted with the westerlies since the late Oligocene (Wang et al., 2020) and caused a reorganization of Central Asian climate during the Neogene (e.g. Bougeois et al., 2018; Caves Rugenstein & Chamberlain, 2018; Hellwig et al., 2018). Growth of the Terskey range formed a topographic barrier during the Miocene, placing the Issyk-Kul

basin area in a windward position with respect to the path of the westerlies and local topography (Figure 1; Macaulay et al., 2016). Formation of an orographic barrier typically requires relief of ca. 1300–2000 m (Bookhagen & Burbank, 2010; Bookhagen & Strecker, 2008).

Precipitation in the Tian Shan is seasonally influenced by interactions between the westerlies and the Siberian High (e.g. Aizen et al., 1997; Prud'homme et al., 2021; Schwarz et al., 2017; Zech, 2012). Moisture, delivered by the monsoon, never consistently reached the Tian Shan and did not influence long-term climate within the range (Caves et al., 2015). The westerlies bring moisture from the North Atlantic, the Mediterranean and the Black Sea (Aizen et al., 2006; Lauterbach et al., 2014). In winter, the Siberian High reaches the Tian Shan and blocks the mid-latitude westerlies, resulting in cold conditions and low precipitation (Aizen et al., 2001; Ricketts et al., 2001).

2.3 | Development of the Issyk-Kul basin

Today, the semiarid Issyk-Kul basin is internally drained, hosting a large lake (ca. 180×60 km with a depth of 668 m). Issyk-Kul means warm lake in the Kyrgyz language; however, to prevent confusion in this paper, we refer to the basin as Issyk-Kul and to the lake as lake Issyk-Kul. During past lake highstands, the lake has been periodically externally drained via the northward-flowing Chu river, which flows through the Boom gorge (Figure 1b; e.g. Gebhardt et al., 2017; Rosenwinkel et al., 2017). Maximum precipitation is recorded in spring and summer (Aizen et al., 2001). As indicated by palynologic data, during the Cenozoic, the basin underwent aridification and forests were gradually replaced by steppe and desert elements (Grigina & Fortuna, 1981). Since the late Pleistocene, the vegetation is similar to modern flora (Fortuna et al., 2017; Grigina & Fortuna, 1981). Subsurface sedimentological data from the eastern side of the basin suggest that a local shallow lake existed in the Miocene and expanded westward in the late Pliocene (Grigina & Fortuna, 1981; Voskresenskaya, 2013; Voskresenskaya & Leflat, 2015). However, to date, there are only sparse data with well-established age constraints indicating when or how the lake first formed or when the present climate was established.

The late Mesozoic–Cenozoic sedimentary deposits of the Issyk-Kul basin are divided into four sedimentary groups: the Kokturpak, Shamsi, Chu and Sharpyl Dak groups (Abdrakhmatov et al., 2001). The Kokturpak group is the oldest in the Issyk-Kul basin with a late Cretaceous to Eocene age based on palynology (Fortuna et al., 1994) and comprises paleosols, lacustrine and poorly sorted low-energy fluvial sedimentary rocks. The unconformably overlying Shamsi group contains

reddish conglomerates deposited in a high-energy regime; the deposits are coarser and better rounded than those in the underlying group. Palynologic data imply an Oligocene–early Miocene age of the group (Fortuna et al., 1994). The first magnetostratigraphic age models of the Shamsi group suggest depositional ages of 22.8 to 13.3 Ma or 22.1 to 11.1 Ma in the Jeti Oguz section and 26.0 to 16.2 Ma or 25.2 to 11.0 Ma in the Chon Kyzylsu section (Figure 1c; Wack et al., 2014). More recent paleomagnetic results (Roud et al., 2021) from these two sections allowed for a re-evaluation of the age models. The revised magnetostratigraphic age models from Roud et al. (2021) suggest a depositional age of 22.4 to 8.5 Ma in the Jeti Oguz section and 17.3 to 7.5 Ma in the Chon Kyzylsu section. Deposits of the stratigraphically younger Chu group are finer-grained than the older Shamsi group. The Chu group contains beige and yellowish fluvial sandstones and siltstones, as well as conglomerates deposited by high-energy river systems. The estimated age of the Chu group in the Chu basin is late Miocene–early Pliocene; lithostratigraphic correlation implies the same age range in the Issyk-Kul basin (Bullen et al., 2001; Omuraliev & Omuralieva, 2004). The Sharpyl Dak group overlies the Chu group gradually or with an unconformity and represents poorly sorted, very coarse conglomerates. Palynologic data implies a late Pliocene–early Pleistocene age of the group (Fortuna et al., 1994; Grigina & Fortuna, 1975). The first magnetostratigraphic age models for the Chu group and Chu–Sharpyl Dak transition were proposed by Roud et al. (2021). In that study, the depositional age of the Chu group in the Ak Terek section is interpreted to be 6.3 to 2.8 Ma. Two possible age models were proposed for the Chu–Sharpyl Dak deposits in the Kaji Say section. The first one is 12.7 to 9.5 Ma. The second option implies a hiatus in the middle of the section, with ages of 7.0 to 5.1 Ma for the lower part and 3.0 to 2.4 Ma for the upper part.

3 | MATERIALS AND METHODS

3.1 | Sedimentological descriptions

Sedimentary sequences were described at five localities around lake Issyk-Kul during fieldwork in 2016 and 2017: Kaji Say and Ak Terek on the southern side, which were previously dated by Roud et al. (2021) using magnetostratigraphy, Jergalan on the eastern side and Cholpon Ata and Toru Aygir on the northern side (Figure 1c). The work included detailed descriptions of composition, bedding structures, paleocurrent directions, conglomerate clast counts and facies interpretations. Paleocurrent

directions were defined by measuring the orientations of imbricated conglomerate clasts and cross-bedding. Conglomerate clast counts were performed by identifying at least 100 clasts within a 1 m^2 space in suitable areas of the sections.

3.2 | $^{26}Al/^{10}Be$ isochron burial dating

We use the technique of terrestrial cosmogenic nuclide isochron burial dating to determine the age of the sedimentary sequences. Terrestrial cosmogenic nuclides are isotopes produced in silicate minerals by the interactions of secondary cosmic rays with the upper few metres of the Earth's surface (Lal, 1991; Schaefer et al., 2022). Quartz is the main target mineral from which the concentration of cosmogenic radionuclides ^{26}Al and ^{10}Be are most routinely measured. Burial dating is based on the radioactive decay of ^{26}Al and ^{10}Be isotopes in rocks that are completely shielded from new production. The concentrations of ^{26}Al and ^{10}Be in a sample are proportional to the duration of exposure (Granger & Muzikar, 2001). The ^{26}Al is produced faster than the ^{10}Be. Although the exact $^{26}Al/^{10}Be$ production ratio is still debated (see Corbett et al., 2017 and references therein; Halsted et al., 2021), the consensus value, widely used in the literature, is 6.75:1 (Balco et al., 2008). Therefore, for consistency with other work, we use the latter in our calculations here. The two isotopes decay at different rates according to their half-lives: 0.717 m.y. for ^{26}Al (Norris et al., 1983) and 1.387 m.y. for ^{10}Be (Chmeleff et al., 2010; Korschinek et al., 2010). When sediments are buried and completely shielded from cosmic radiation, there is no new isotope production and the initial $^{26}Al/^{10}Be$ ratio, which is equal to the production ratio, decreases. Assuming that sediments were rapidly buried after deposition and minimally re-exposed to new production prior to collection, the half-lives of the two nuclides and their initial production rate ratio (above) can be used to calculate the time of burial. The lower the ratio and concentrations, the longer the duration of burial. This assumption is the basis for conventional burial dating that requires the measurement of a single $^{26}Al/^{10}Be$ ratio from a clast or an amalgamated sand sample in order to provide a meaningful age (Granger & Muzikar, 2001).

In tectonically active areas like the Tian Shan, ideal burial conditions rarely occur. Sediments may experience post-burial production that can alter the inferred burial age. Post-burial nuclide production occurs if the overlying deposits are not thick enough (approx. <30 m)—and therefore material is not completely shielded from incoming cosmic radiation—or when sediments are brought close to the surface after the initial deposition and burial due to erosion, river incision or other factors. Post-burial nuclide

production will increase nuclide concentrations and ratios and result in seemingly younger burial ages. Also, the sediments are affected by a complex combination of exposure and material mixing prior to burial, which can lead to obtaining inherited concentrations of nuclides (Codilean & Sadler, 2021). In settings where conventional burial dating assumptions are violated, a relatively new method—isochron burial dating—may be used to obtain a reliable burial age (Balco & Rovey, 2008; Erlanger et al., 2012; Knudsen et al., 2020).

The isochron burial dating method does not require information about depth, exposure and post-burial nuclide production (Balco & Rovey, 2008). Rather, it requires a set of quartz-bearing clasts from one depositional horizon that was sufficiently shielded such that post-burial production is minimized (but not necessarily eliminated). Each clast in the depositional horizon will record the same post-burial history but different preburial exposure histories as the clasts likely originated from different source areas. The ^{26}Al and ^{10}Be concentrations form an isochron on a ^{10}Be-^{26}Al plot, and the slope of this isochron will depend only on the burial age. The isochron slope reflects the deviation from the ^{26}Al/^{10}Be production rate and will depend on the half-lives of the nuclide pair and on the duration of decay. Therefore, the burial age (t_b) may be calculated as shown by Balco and Rovey (2008):

$$t_b = -\ln\left(R_M / R_{\text{init}}\right) / \left(\lambda_{26} - \lambda_{10}\right)$$

where R_M is the slope of the isochron; R_{init} is the ^{26}Al/^{10}Be production ratio; λ_{26} and λ_{10} are the decay constants of ^{26}Al and ^{10}Be, respectively.

To confirm and improve the magnetostratigraphic age models from Roud et al. (2021), we dated the Kaji Say and Ak Terek sections. We also attempted to date the sections on the northern and eastern sides of the basin. We therefore collected a total of ten samples (one sample is one isochron) of individual clasts and amalgamated sand (250–500 μm grain size) from four localities—the Kaji Say, Ak Terek, Jergalan and Cholpon Ata sections (Figure 1c). Four samples were taken in the Kaji Say section: PET-L and PET-U from the lowermost part of the section, PET-QTS-PIT from the Chu-Sharpyl Dak transition and PET-QTS-L from the uppermost Sharpyl Dak. Two samples were taken in the Ak Terek section: AKT-U from the uppermost Chu and AKT-Q from the lower Sharpyl Dak. Two samples were taken in the Jergalan section: JGL-2 from the Chu deposits and JGL17 from the Chu-Sharpyl Dak transition. Two samples were taken in the Cholpon Ata section: CA17-6 from the upper Chu part and CA17-1 from the lower Sharpyl Dak.

At each of the ten sampled locations, we collected about ten clasts. Clasts were chosen based on their size,

lithology and inferred amount of quartz present. Our aim was to collect diverse, quartz-rich lithologies, in order to capture different preburial histories. All collected clasts were approximately 10–12 cm in diameter. Smaller clasts would not contain enough quartz and larger clasts could have been subject to self-shielding. The clasts were collected from areas where modern production is minimized due to shielding. Due to very low quartz yield in some of the clasts, only three to six clasts were analysed per isochron. At six of the sampled locations, in addition to the individual clasts, we also collected an amalgamated sand sample as an independent test of the isochron and assumptions about shielding and post-burial production (the ^{26}Al-^{10}Be of the sand sample should plot on the isochron defined by the individual clasts if assumptions are met).

The initial sample preparation (crushing and sieving) was done at the University of Potsdam, Germany. Quartz was isolated and purified at the University of Wollongong, Australia, following procedures described in Kohl and Nishiizumi (1992), using froth flotation to separate feldspars from quartz. Be and Al were separated at the University of Wollongong following procedures described in von Blanckenburg et al. (1996) with the modification that Al was separated from Be and Ti using pH-sensitive precipitation before Be cation exchange chromatography (Child et al., 2000). Samples were spiked with ≈300 μg of ^{9}Be from a low-level beryllium carrier solution added prior to complete HF dissolution. ^{10}Be/^{9}Be and ^{26}Al/^{27}Al ratios were measured using the 6MV SIRIUS facility at the Australian Nuclear Science and Technology Organisation (ANSTO; Wilcken et al., 2019, 2021). The native Al concentrations of the samples ranged from 47 to 490 ppm (median = 96 ppm; average = 124 ppm) and were determined via ICP-OES with a precision of 3%–4% (Fujioka et al., 2015). ^{10}Be/^{9}Be ratios were normalized to the KN-5-2 and KN-5-3 (Nishiizumi et al., 2007) standards and ^{26}Al/^{27}Al ratios were normalized to the KN-4-2 (Nishiizumi, 2004) standard. Analytical uncertainties for the final ^{10}Be and ^{26}Al concentrations (atoms g^{-1}) include AMS measurement uncertainties (the larger of counting statistics or standard deviation of repeats and blank corrections) in quadrature with 1%–2% for ^{10}Be and 2%–3% for ^{26}Al standard reproducibility (depending on the individual AMS measurement conditions), 1% uncertainty in the ^{9}Be carrier concentration and 4% uncertainty in the ICP-OES Al measurements.

3.3 | Thin-section petrography

Petrographic analysis was performed using a polarized light microscope on 27 sandstone and lacustrine

micrite thin sections from Kaji Say and 16 sandstone thin sections from Ak Terek to evaluate the diagenetic and palustrine alteration of the sediment sequences. Compaction and cementation of fluvial-alluvial samples as well as the amount of recrystallization and pedogenic alteration of lacustrine micrite samples were evaluated.

3.4 | Stable isotope analysis

To reconstruct paleoenvironmental conditions, a total of 122 carbonate samples were collected for stable isotope analysis: 53 samples from the Kaji Say section and 69 from the Ak Terek section. The Kaji Say samples consist of pedogenic nodules (17 samples), sparitic cement in sandstones (16 samples), micrite in lacustrine mudstone (10 samples) and micrite in lacustrine marl and siltstone (10 samples). The majority of the Ak Terek samples are pedogenic nodules (64 samples), with only 5 samples of sparitic cement in sandstones.

Stable isotope values were measured at the Joint Goethe University—Senckenberg BiK-F Stable Isotope Facility at Goethe University Frankfurt, Germany. The finest parts of the samples were drilled; the powder was digested in orthophosphoric acid and analysed using a Thermo MAT 253 mass spectrometer interfaced with a Thermo GasBench II. The analytical procedures follow Spötl and Vennemann (2003). Raw isotopic ratios were calibrated against NBS 18, Merck and Carrara marble standards. All isotope values are relative to the Pee Dee Belemnite (V-PDB). Analytical uncertainties are typically smaller than 0.10 ‰ ($\delta^{18}O$) and 0.07 ‰ ($\delta^{13}C$).

4 | RESULTS

## 4.1 | Sedimentary sequences

4.1.1 | Kaji Say section

The 700-m-thick Kaji Say section is located in the Tossor–Kaji Say area and comprises the Chu and Sharpyl Dak groups (Figure 1c). Paleocurrent directions indicate predominantly NW flow directions in the section. The Chu group deposits can be divided into two depositional units (Figure 2). The lower unit is 450 m thick; it is formed of alternating grey rounded conglomerates with clasts of mainly cobble and boulder size (Figure 3a), red angular conglomerates with clasts of mainly gravel and cobble size (Figure 3b), grey and red sandstones, and beige siltstones. The upper unit is 190 m thick and comprises alternating red angular conglomerates with clasts of mainly gravel

and cobble size, beige pebbly sandstones, blue calcareous mudstones, white marls, calcareous siltstones and marly sandstones (Figure 3c–e). The red and grey colours represent different sedimentary lithologies. Red conglomerates are matrix-supported and composed of clasts of porphyry with quartz phenocrysts in a fine-grained groundmass. Grey conglomerates are clast supported and consist predominantly of granite clasts. In order to measure well-exposed outcrops, the Kaji Say section was divided into western and eastern transects, situated in different valleys (Figure 4). Continuous beds can be followed between the two transects; no more than 10 m of strata was omitted. Bedding dips indicate the presence of a fold: ca. 10°–25° (dip direction is ca. 350–355 N) at the base of the section (0–245 m), ca. 75° (ca. 0 N) at the top of the lower Chu unit (ca. 245–480 m), ca. 25°–35° (ca. 5–10 N) in the upper Chu unit (ca. 480–640 m), and ca. 15° (ca. 5–10 N) at the top of the section (Figure 4).

In the lower Chu unit, the red and grey conglomerates laterally and stratigraphically change into sandstones and siltstones. Grey and red beds alternate and have sharp boundaries. Mixed coarse grey and greyish-red sandstones with red gravel lenses occur in the middle part of the section. Grey granitic channel lag conglomerates are generally coarser than the red ones, and grey deposits are better sorted and better cemented. Sandstones are cross-bedded; siltstones are laminated and contain pedogenic calcrete nodules and lenses of poorly sorted pebbly and sandy gravel. In the upper Chu unit, white marly sandstones are fine, well sorted and well cemented; beige sandstones are coarse and contain lenses of red gravel. Blue calcareous mudstones contain rare ostracode shells (see petrography section, below); calcareous siltstones contain rare pedogenic calcrete nodules and display soft sediment deformation and slump folding directed towards the lake. The beds in the upper Chu unit thicken to the northwest. The Chu–Sharpyl Dak transition is gradational. Sharpyl Dak deposits are 60 m thick in the section; they consist of 10–20-m-thick red conglomerate beds of angular gravel and cobble clasts with poorly sorted matrix, as well as beige sandstones, white marls and white calcareous siltstones.

Clast counting was performed at 4 localities in the lower Chu unit: 85, 144, 320 and 411 m. Grey conglomerates consist predominantly of white and red granite clasts with a minor occurrence of volcanic rocks, shale, quartzite, pegmatitic quartz, metamorphic sandstone and sandstone clasts. Red angular conglomerates show the prevalence of red porphyry clasts with quartz phenocrysts, and the presence of granite, quartzite, pegmatitic quartz, volcanic and metamorphic sandstone clasts. Clast compositional data for this and the other four localities are shown in the Supporting Information.
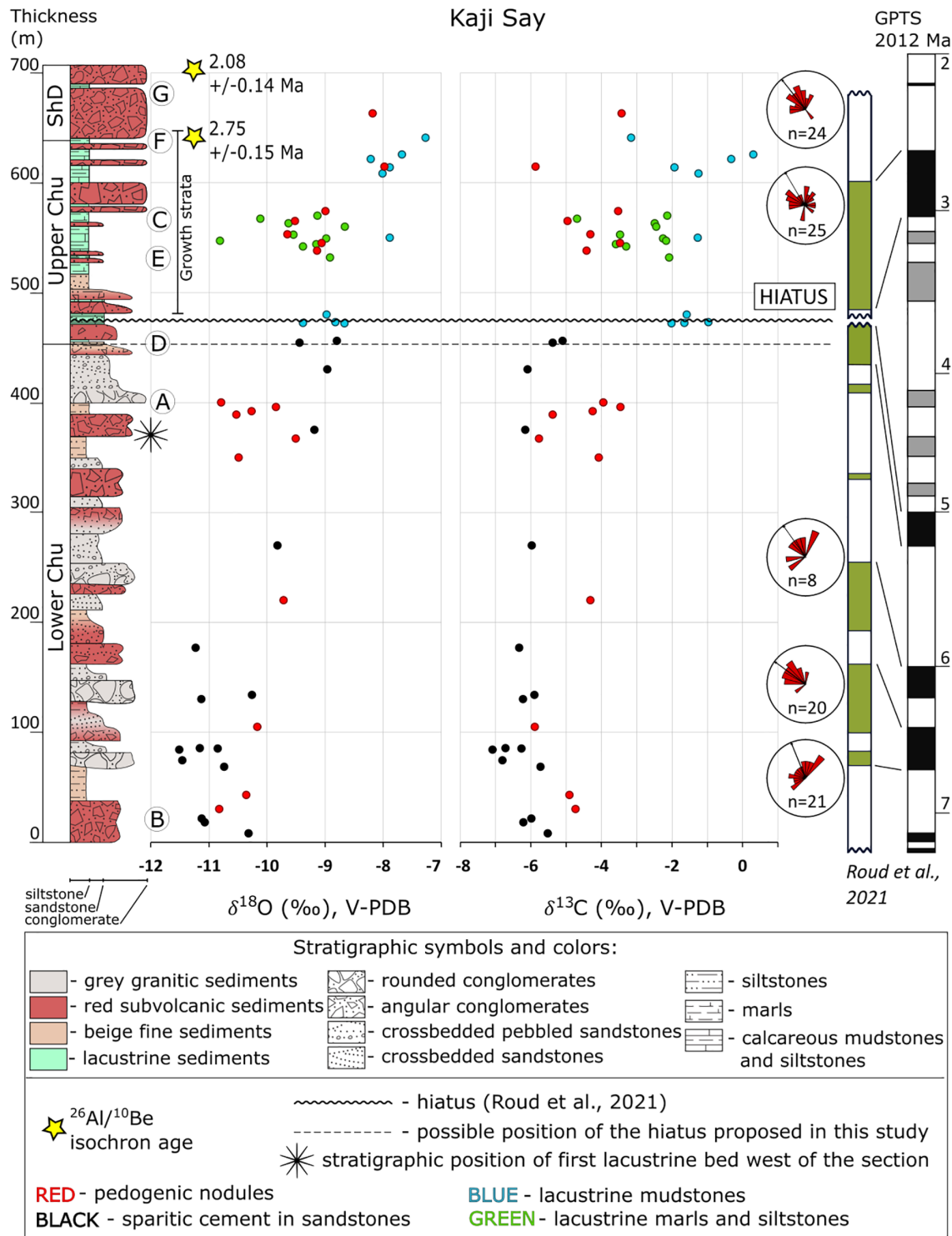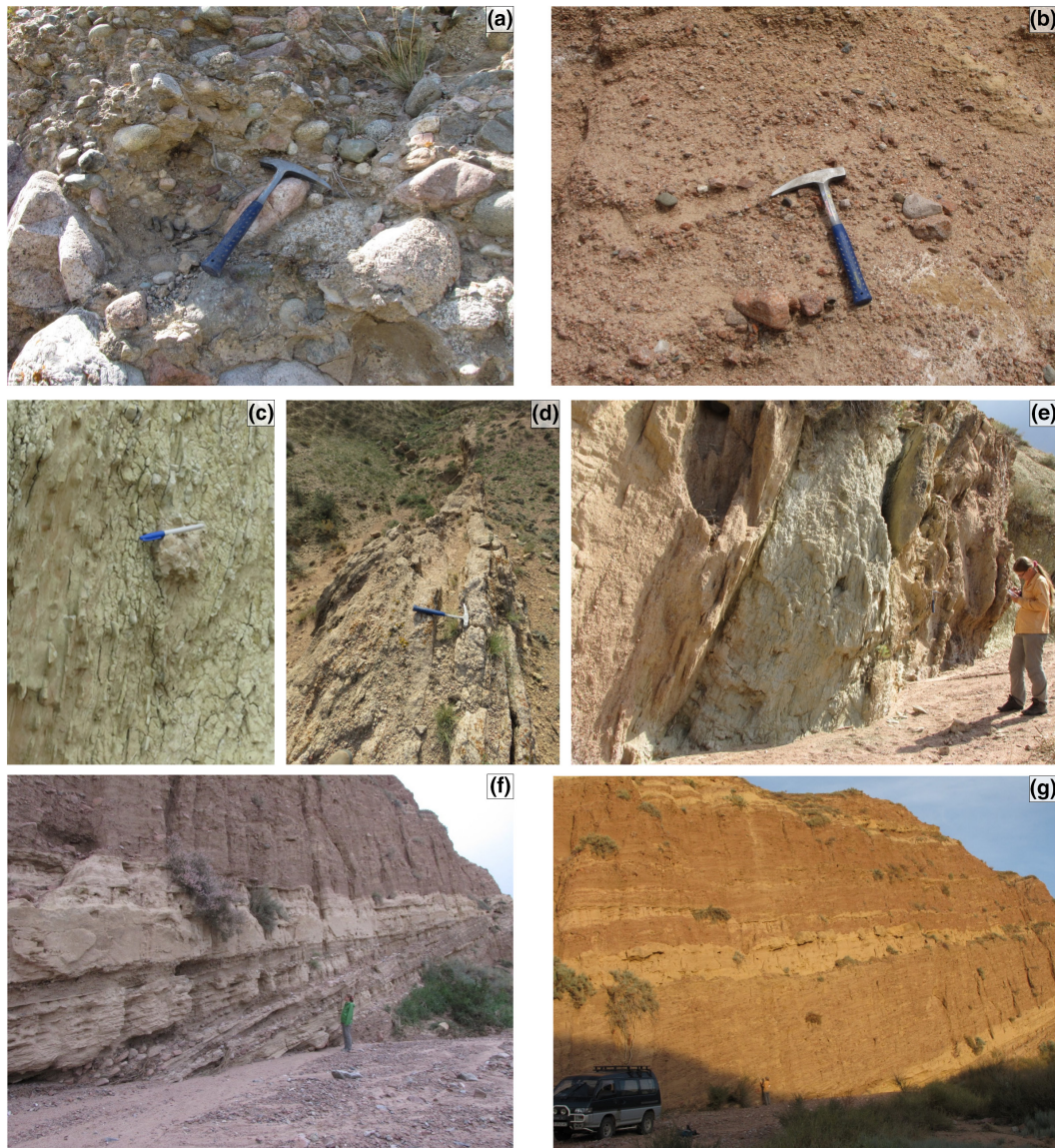
FIGURE 2 Kaji Say stratigraphic section (location shown in Figure 1) with ^{26}Al/^{10}Be isochron burial ages, rose diagrams of paleocurrent flow directions (black arrow shows the main vector) and stable isotopic values plotted against the magnetostratigraphic age model of Roud et al. (2021). ShD is Sharpyl Dak. A–G show stratigraphic positions of photographs, represented in Figure 3.

4.1.2 | Ak Terek section

The Ak Terek section is a 500-m-thick sequence of the Chu group, located in the southwestern part of the basin (Figure 1c; see Figure S1 for detailed location of the section; detailed geological maps of the Ak Terek section area are available in Roud et al., 2021 and Burgette et al., 2017). The deposits represent a series of depositional cycles with normal gradation: grey conglomerates are interbedded with well-sorted

FIGURE 3 Characteristic field photographs from the Kaji Say section. Stratigraphic positions are shown in Figure 2; locations are shown in Figure 4. (a) Grey granitic conglomerates. Hammer for scale. (b) Angular red gravel conglomerates. Hammer for scale. (c) Lacustrine sediments. Pen for scale is 15 cm long. (d) Sandstones of the beach facies, which mark the beginning of lacustrine deposition. Hammer for scale. (e) Interbedding of lacustrine (greenish-white) and alluvial (beige) deposits. Person for scale is 170 cm tall. (f) Growth strata. Person for scale is 170 cm tall. (g) Deposits of the Sharpyl Dak sedimentary group. Car for scale is ca. 2 m high.

sandstones, beige siltstones and mudstones (Figure 5). The top of the section represents the uppermost Chu deposits close to the overlying coarse conglomerates of the Sharpyl Dak group. Paleocurrent measurements indicate predominantly northeast flow directions. Well-rounded conglomerate clasts are of gravel and cobble size (Figure 6a). Granite is the dominant source rock type in the lowermost part of the section. Metamorphic sandstone, volcanic rocks and quartzite clasts are also found.

In the lowermost part of the section, mudstone beds contain layers of poorly developed paleosols and slickensides, with a gradual upsection increase in palaeosol nodule abundance (Figure 6b). In the uppermost 80 m of the section, the thickness of fine deposits and the amount of pedogenic nodules decrease. Two prominent 30-cm-thick gypsum layers were found at 430–440 m of the section, while older deposits of the section contain only rare thin lenses of gypsum.

4.1.3 | Jergalan section

The Jergalan section is located in the eastern part of the Issyk-Kul basin (Figure 1c). We could not describe the sedimentary sequence in detail because of the steep
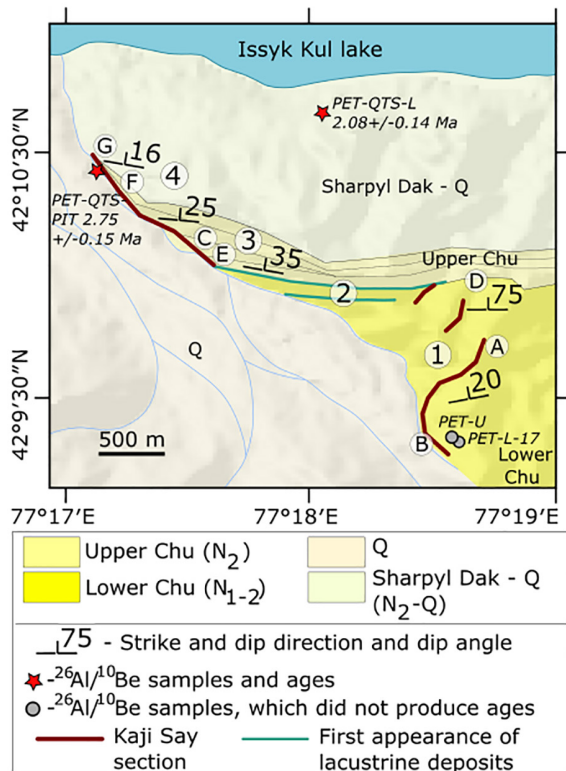
FIGURE 4 Kaji Say section area (location shown in Figure 1). Sedimentary units are mapped using Bing Maps satellite imagery and topography based on SRTM30 digital elevation data. A–G show locations of the corresponding photographs, represented in Figure 3. 1—Eastern transect of the section showing shallow dips in the stratigraphically older part and vertical dips in the stratigraphically younger part. This dip pattern defines a fold; cross section shown in Roud et al. (2021). 2—First lacustrine beds in the area. The stratigraphically older lacustrine bed does not reach the measured section and is not included in the description (Figure 2). The stratigraphically younger bed represents the first lacustrine beds included in the description. 3—Growth strata (photograph shown in f). 4—Western transect of the section with shallow dips. Stratigraphic units in the legend: N_{1-2}—Late Miocene–early Pliocene; N2—Pliocene; N2-Q—Pliocene–Quaternary; Q—Quaternary.

relief and poor exposure due to numerous landslides. The sequence crops out in two cliffs (Figure 7a). The lower part of the section in cliff 1 represents mostly sandstones and fine-grained material. The amount and thickness of conglomerates gradually increase upsection. The conglomerates are massive, matrix-supported and interbedded with thin sandstone beds. Conglomerates were deposited in channel structures incising into finer beds. The beds dip gently to the west. We estimated the most probable position of the Chu–Sharpyl Dak transition prior to sampling for ^{26}Al/^{10}Be isochron burial dating. The contact between lower fine-grained sedimentary rocks and upper conglomerates

in cliff 2 is visually similar to the Chu–Sharpyl Dak transition in the Kaji Say section and might also represent the beginning of the Sharpyl Dak conglomerate accumulation (Figure 7d). Sharp contacts are exposed in the uppermost parts of both ca. 200 m high cliff walls (Figure 7b,c). The gently dipping beds are truncated by almost flat-lying boulder-bearing conglomerates. These conglomerates cut down into the underlying units. Clast count and paleocurrent measurements were performed at the position of sample JGL17 at the base of the gently dipping conglomerates above the lower part of the section. Conglomerates are mainly composed of clastic sedimentary rocks, as well as clasts of granites, volcanic rocks, quartzite and quartz. Paleocurrent measurements suggest south-directed transport.

4.1.4 | Toru Aygir section

The 24-m-thick Toru Aygir section is situated in the northwestern side of the basin (Figure 1c; detailed geological map of the Toru Aygir area is shown in Figure S2). The lower part consists of brown fine and coarse sandstones, with interbeds of granitic pebbles and gravel and thin lenses of siltstones. The upper part consists of a series of normally graded conglomerates deposited in channel structures and well-sorted sandstones (Figure 6c; stratigraphic log is shown in Figure S3). The conglomerates and sandstones gradually change into one another along strike. Paleocurrent measurements show predominantly south-directed transport (Figure 1c and Figure S3). The most abundant rock type among the conglomerate clasts is subvolcanic rocks with plagioclase phenocrysts. Clasts of granites, mafic igneous rocks and volcanic rocks are also found.

4.1.5 | Cholpon Ata section

The 20-m-thick Cholpon Ata section is situated on the northern side of the basin (Figure 1c; detailed geological map of the Cholpon Ata area is shown in Figure S2). It consists of rounded conglomerates, siltstones and beige well-sorted cross-bedded fine to coarse sandstones with lenses of granitic pebbles and cobbles (Figure 6d; stratigraphic log is shown in Figure S4). Interbeds of well-cemented and well-sorted sandstones appear every ca. 1.5 m. Thickness of conglomerate beds varies along the section from 20 cm to 1.5 m. Paleocurrent directions show predominantly southward flow directions (Figure 1c and Figure S4). Granites are dominant among conglomerate clasts besides clasts of phyllite, volcanic rocks and clastic sedimentary rocks.
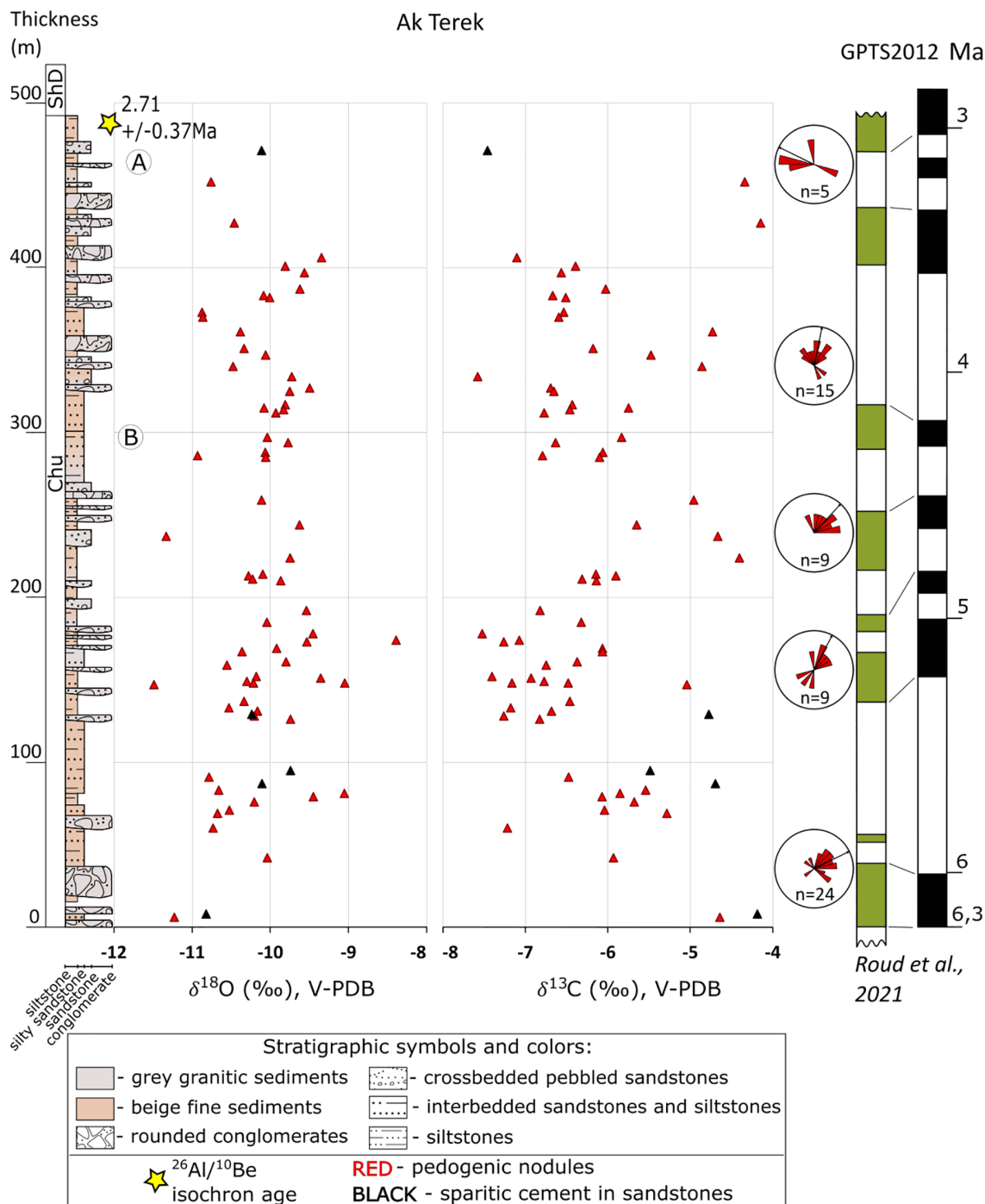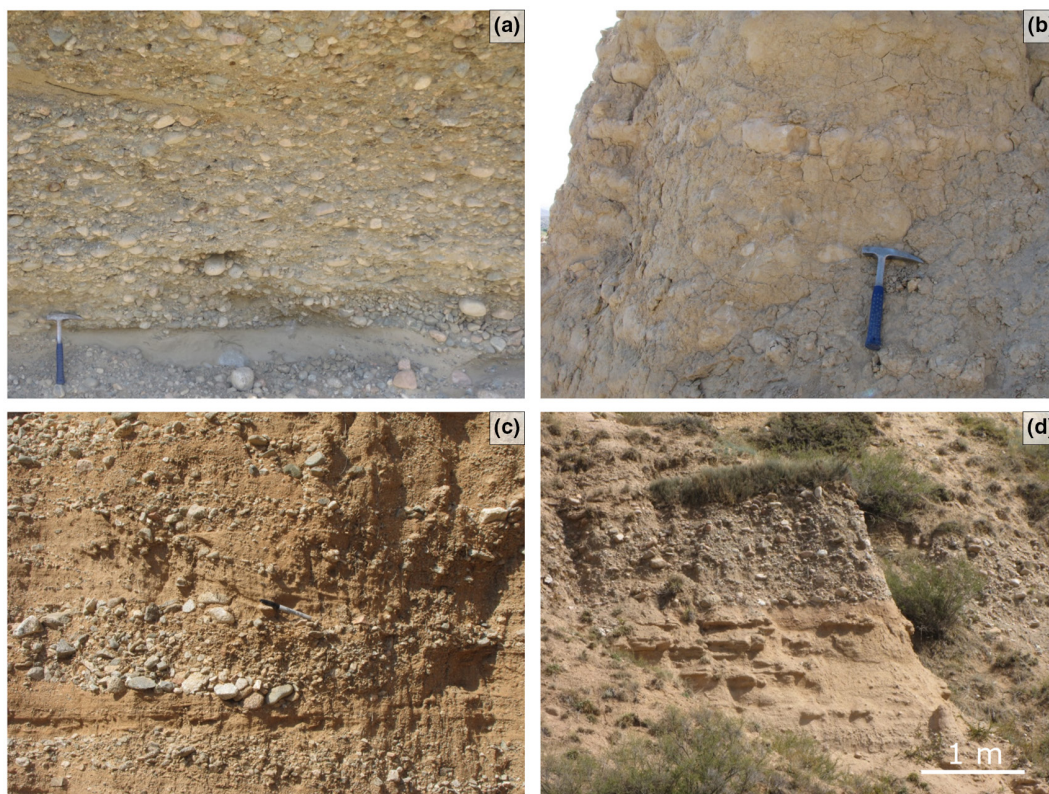
FIGURE 5 Ak Terek stratigraphic section (location shown in Figure 1) with a ^{26}Al/^{10}Be isochron burial age, rose diagrams of paleocurrent flow directions (black arrow shows the main vector) and stable isotopic values plotted against the magnetostratigraphic age model of Roud et al. (2021). ShD is Sharpyl Dak. A and B show stratigraphic positions of photographs, represented in Figure 6.

4.2 | ^{26}Al/^{10}Be isochron burial dating

Five of the ten collected samples yielded usable results (Figure 8). The ^{26}Al and ^{10}Be concentrations of the other samples do not form an isochron—either due to the low number of datapoints (e.g. PET-L and PET-U) or due to burial ages exceeding the useful time range of the ^{26}Al–^{10}Be isotope pair (e.g. CA17-1 and CA17-6)—and so burial ages

could not be calculated with confidence for these samples. In the Kaji Say section, the Chu–Sharpyl Dak ^{26}Al/^{10}Be-isochron-inferred transition age is 2.75 ± 0.15 Ma (sample PET-QTS-PIT; Figure 8e) and the top of the section in the Sharpyl Dak deposits is 2.08 ± 0.14 Ma (sample PET-QTS-L; Figure 8d). In the Ak Terek section, the upper Chu deposits close to the overlying Sharpyl Dak provide an age of 2.71 ± 0.37 Ma (sample AKT-U; Figure 8c).

FIGURE 6 Characteristic field photographs from the Ak Terek (a,b), Toru Aygir (c) and Cholpon Ata (d) sections. Stratigraphic positions of A,B are shown in Figure 5; geographical locations of A,B are shown in Figure S1. Stratigraphic position of C is shown in Figure S3. Stratigraphic position of D is shown in Figure S4. (a) Conglomerates in the Ak Terek section. Hammer for scale. (b) Floodplain deposits with palaeosol horizons in the Ak Terek section. Hammer for scale. (c) Conglomerate channels in the Toru Aygir section. Pen for scale is 15 cm long. (d) Conglomerate channels and floodplain deposits in the Cholpon Ata section.

In the Jergalan section, sample JGL17 yielded an age of 4.26 ± 0.44 Ma for the presumable Chu–Sharpyl Dak transition (Figure 8h). In the case of JGL-2, the obtained ^{26}Al concentrations were statistically indistinguishable from the procedural blank. Given that no ^{27}Al carrier solution was added to the JGL-2 samples during processing, correcting for ^{26}Al blank is not strictly necessary (see Wilcken et al., 2021 for more details). Using the raw (i.e. not blank-corrected) ^{26}Al, JGL-2 produces an age of 4.76 ± 0.82 Ma (Figure 8i2).

4.3 | Petrographic study of thin sections

Thin sections of fluvial-alluvial sandstones from the Kaji Say and Ak Terek sections show mechanical compaction of sandstones, which resulted in point to concavo–convex contacts, as well as ductile deformation of detrital mica (Figure 9a,b). Detrital feldspar grains are partially corroded by calcite cement. The Ak Terek and Kaji Say sandstone samples are predominantly arkose and cemented by calcite, which consists mostly of sparitic blocky cement (Figure 9a). Poikilotopic calcite cement is found

in samples of fluvial-alluvial sandstones of the Ak Terek section and the lower Chu unit of the Kaji Say section (Figure 9b). Sandstones from the upper Chu unit of the Kaji Say section are not compacted; they contain primary carbonate micrite and microsparite cement, as well as patchy sparitic cement (Figure 9c). Lacustrine samples are composed of primary dense micrite and microsparite (Figure 9d). Some lacustrine samples contain ostracode shells, desiccation cracks and pores with alveolar textures filled with sparitic cement (Figure 9d,e).

4.4 | Oxygen and carbon isotope ratios

δ^{18}O values of Kaji Say samples (Figure 2) range from $-11.5‰$ to $-7.3‰$ (PDB), with an average value of $-9.6 \pm 1.1‰$ (1σ); δ^{13}C values range from $-7.1‰$ to $0.3‰$ (PDB), with an average value of $-4.1 \pm 1.9‰$ (1σ). Samples of pedogenic nodules were taken throughout the whole section, with average values of δ^{18}O $= -9.7 \pm 0.8‰$ and δ^{13}C $= -4.5 \pm 0.8‰$. Samples of carbonate cement in fluvial sandstones were taken from the lower Chu unit, with average values of δ^{18}O $= -10.4 \pm 0.9‰$ and δ^{13}C $= -6.1 \pm 0.5‰$.
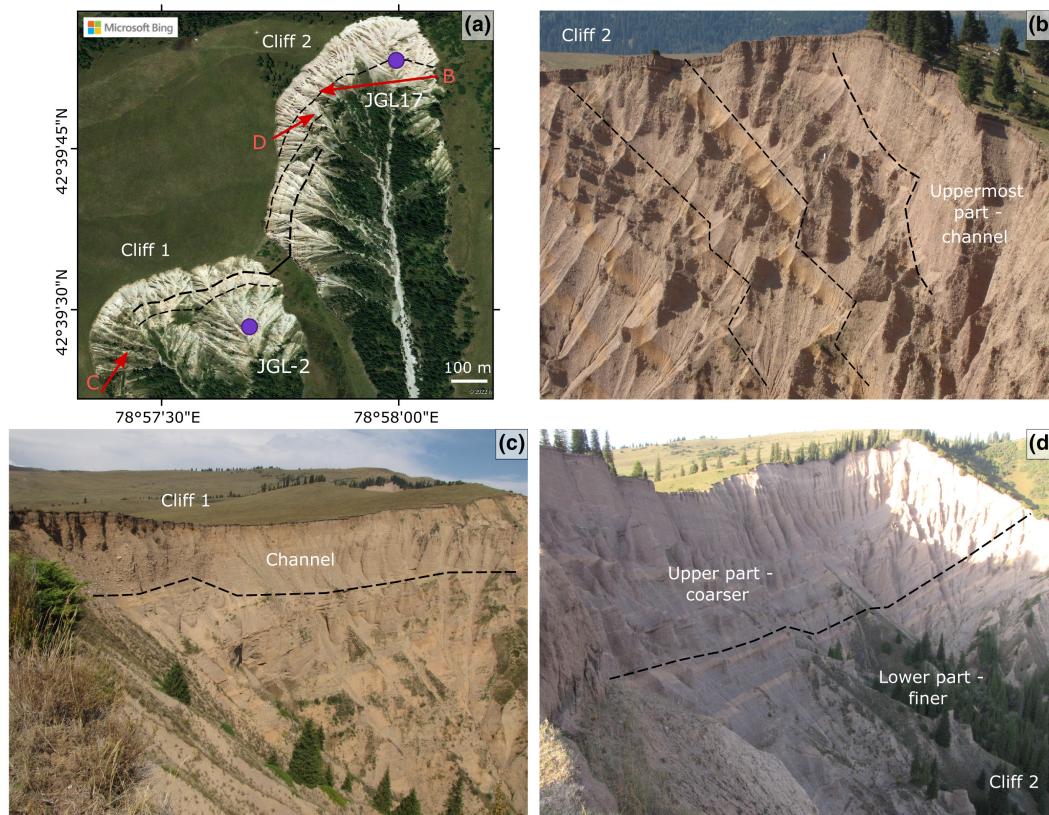
FIGURE 7 Satellite imagery and field photographs of the Jergalan section (location shown in Figure 1). (a) Bing Maps image of the section showing the two cliffs and positions of the ^{26}Al/^{10}Be isochron burial dating samples. Lower (finer) part of the section outcrops in cliff 1; cliff 2 represents the transition between the lower and upper (coarser) parts of the section. Dashed lines show bedding and correlation of beds between the two cliffs. Red arrows show the view directions of the corresponding photographs b–d. (b) Uppermost part of the section with angular unconformity and a channel structure on top of the cliff 2. (c) Angular unconformity and a channel structure on top of the cliff 1. (d) Gradational transition between the lower (finer) and upper (coarser) parts. Dashed line shows the estimated beginning of the Sharpyl Dak group deposition.

Samples of lacustrine marl, siltstone and mudstone were taken from the upper Chu unit, with average values of $\delta^{18}O = -8.8 \pm 0.9‰$ and $\delta^{13}C = -2.1 \pm 1.2‰$.

$\delta^{18}O$ values of Ak Terek samples (Figure 5) range from $-11.5‰$ to $-8.4‰$ (PDB), with an average value of $-10.1 \pm 0.6‰$ (1σ); $\delta^{13}C$ values range from $-7.6‰$ to $-4.2‰$ (PDB), with an average value of $-6.1 \pm 0.9‰$ (1σ).

Both $\delta^{18}O$ and $\delta^{13}C$ values from the Kaji Say gradually increase upsection, whereas Ak Terek values show no trend, but have a higher variability.

The stable isotope data are provided in the Table S1.

5 | DISCUSSION

5.1 | Depositional age and environment

5.1.1 | Kaji Say

Two magnetostratigraphic age models have been published for the Kaji Say section (Roud et al., 2021). The first option features continuous sedimentation between 12.7 and 9.5 Ma, with an average sedimentation rate of 25 cm. ka^{-1} and the Chu−Sharpyl Dak transition at ca. 10 Ma. The second, preferred option assumes a 2 Ma hiatus in the middle of the section with ages of 7.0–5.1 Ma for the lower part and 3.0–2.4 Ma for the upper part, and average sedimentation rates of 23 and 30 cm.ka^{-1}, respectively. The Chu−Sharpyl Dak transition for the second option is at 2.8–2.6 Ma. The new ^{26}Al/^{10}Be isochron burial ages we obtained from the upper part of the section show that this transition at ca. 640 m in the section is 2.75 ± 0.15 Ma (sample PET-QTS-PIT, Figure 8e), and the Sharpyl Dak sample at the top of the section is 2.08 ± 0.14 Ma (sample PET-QTS-L, Figure 8d). The two sample localities are shown in Figures 2 and 4. Although the isochron burial dating did not work in the lowermost part of the section (samples PET-L and PET-U, Figure 8f,g, respectively; see Figure 4 for position), our two ^{26}Al/^{10}Be isochron burial ages allow for the elimination of the first magnetostratigraphic age model option and stipulate that the age of the Kaji Say section is late Miocene–early Pleistocene (Figure 2).
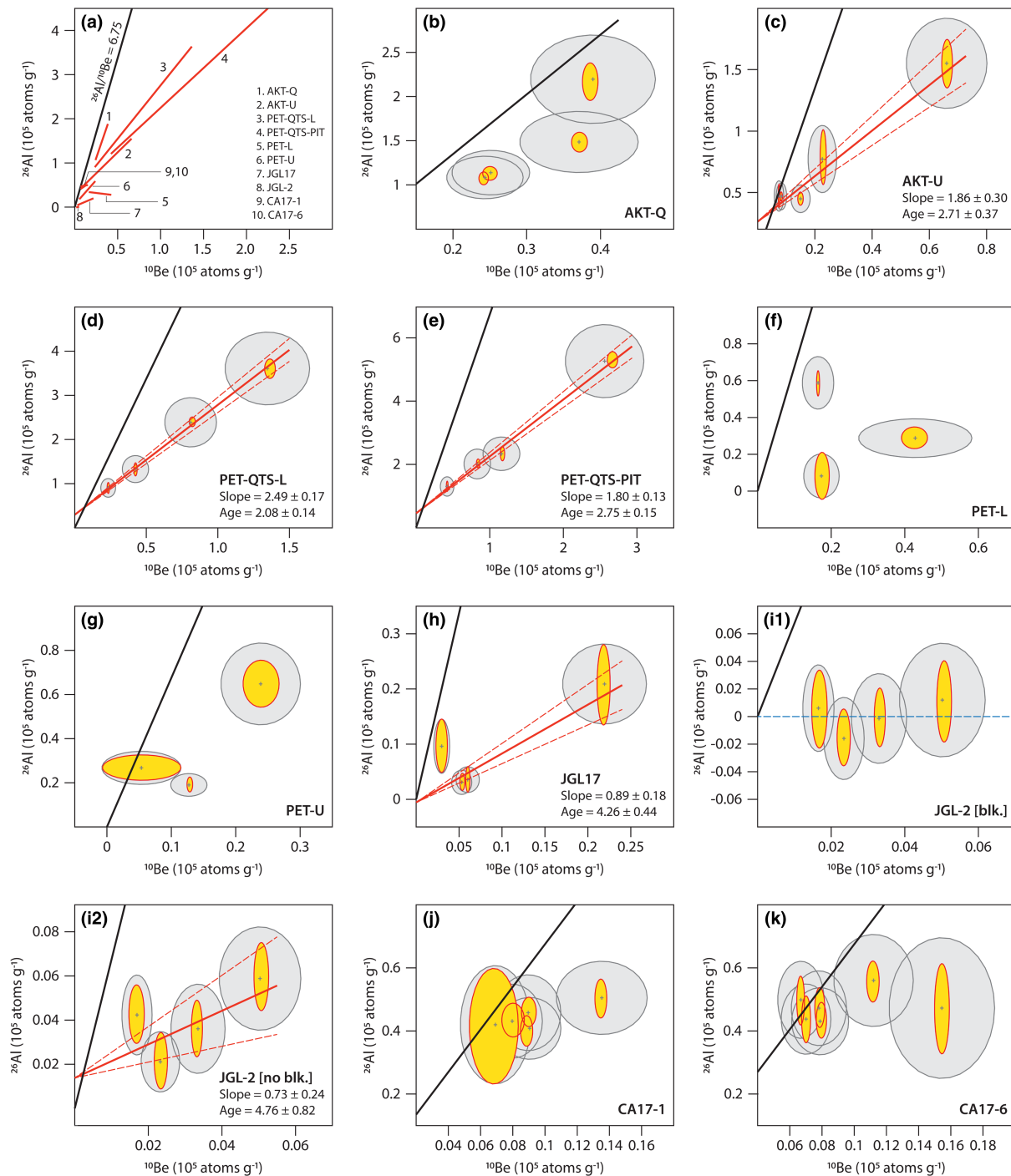
FIGURE 8 Summary of cosmogenic ^{26}Al/^{10}Be isochron burial dating results. (a) Compilation of isochrons (solid red lines) with data points excluded for clarity. Plots (b,c) Ak Terek; (d–g) Kaji Say; (h–i2) Jergalan; (j,k) Cholpon Ata. (b–k) Raw cosmogenic ^{26}Al and ^{10}Be concentrations are shown as yellow 1-sigma error ellipses and linearized concentrations are shown as grey 1-sigma error ellipses. Solid red lines are the error-weighted best fit to the data, and dashed red lines are 1-sigma error bounds. Ages are in Myr. Solid black lines in all plots represent theoretical isochrons for constant production (i.e. no burial) assuming an ^{26}Al/^{10}Be production rate ratio of 6.75. Amalgamated sand samples are not included in the plots. (i1) shows ^{26}Al concentrations at JGL-2 corrected for procedural blank (blue dashed line) and (i2) shows results without blank correction applied to the ^{26}Al data (see text for more details).

Predominantly northwest paleocurrent flow directions indicate that the sediments were sourced from the Terskey range. The lower Chu unit represents a fluvial-alluvial system with overbank deposits, reflecting a braided river system with different source areas within the Terskey range. Rounded well-sorted grey conglomerate clasts (Figure 3a) originated from the widespread granites of the Terskey range. Angular unsorted matrix-supported
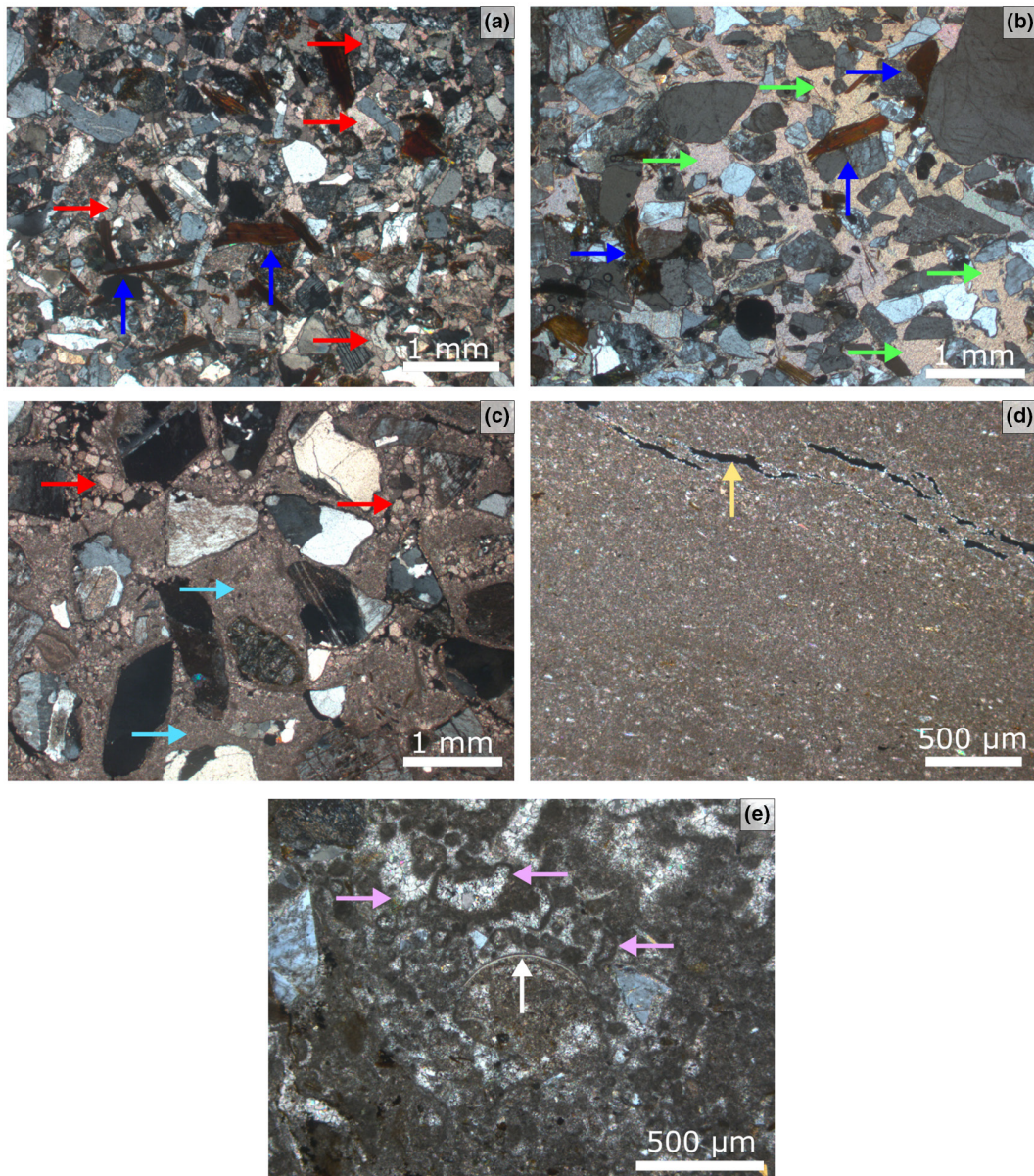
FIGURE 9 Characteristic microphotographs of thin sections from the Kaji Say and Ak Terek sequences under XPL representing early diagenetic and palustrine alteration. (a) Sandstones from the fluvial-alluvial facies, characteristic of the Kaji Say and Ak Terek sections, with sparitic blocky calcite cement (red arrows) and mechanical compaction (dark blue arrows). (b) Sandstones from the fluvial-alluvial facies, characteristic of the Kaji Say and Ak Terek sections, with poikilotopic calcite cement (green arrows) and mechanical compaction (dark blue arrows). (c) Sandstones from the beach facies (Kaji Say) with primary micrite (light blue arrows) and sparitic calcite cement (red arrows). (d) Lacustrine micrite (Kaji Say) with planar cracks (yellow arrow). (e) Lacustrine micrite (Kaji Say) with an ostracode shell (white arrow) and pores with pedogenic alveolar texture (pink arrows) filled with sparitic calcite cement.

red gravel conglomerates (Figure 3b) were presumably delivered from the Taldysui subvolcanic complex, located at the front of the Terskey range around the Kaji Say area. This interpretation is based on the geological map of Kyrgyzstan (scale 1:500,000, VSEGEI, Tursungasiev & Petrov, 2008). The Taldysui subvolcanic complex does not crop out upstream of our other studied sedimentary sections, and they do not contain such clasts.

The characteristics of the red gravel conglomerates indicate that they are debris flow deposits, which represent an alluvial fan with deposits derived from a proximal source area. The grey granitic conglomerates and sandstones were deposited in channel structures and represent the bedload of a braided river with prolonged flows that allowed sorting and normally graded deposition. Conglomerates and well-sorted sandstones mark pulses of high-energy flows. Siltstones represent floodplain deposits that accumulated from sheet flows during strong floods. Pedogenic alteration of the fine sediments is weak, represented by immature horizons of small calcrete

nodules. Their presence indicates changes in the depositional environment with periods of decreased deposition between pulses of conglomerate accumulation (Alonso-Zarza, 2003; Breecker et al., 2009).

The depositional environment changed significantly in the upper Chu unit, which represents a lacustrine environment with a beach, a distal fan delta and periodic rapid intense debris flow deposits of predominantly red angular conglomerates. Lacustrine calcareous mudstones, calcareous siltstones and marls (Figure 3c) were deposited in a shallow lake with low sedimentation rates and decreased clastic input. These are the oldest reported lacustrine deposits in the Issyk-Kul basin above the modern lake level. The occurrence of pedogenic nodules in the lacustrine carbonates and pedogenetic alteration of the lacustrine mudstone, observed in thin sections (see Section 5.2.1), point to repeated lowering of the lake level and exposure of the deposits during dry periods with very slow sedimentation (Alonso-Zarza, 2003; Breecker et al., 2009). The occurrence of thin sandstone lenses within lacustrine marls indicates distal fan delta deposition at the lake margin. The coarse debris flow deposits show that intensified terrigenous input propagated into the lake. Within the measured section, the first beach facies sandstone bed occurs at 450 m, followed by a 5-cm-thick lacustrine calcareous mudstone bed (Figure 3d). Our field observations indicate that lacustrine deposits first appear stratigraphically earlier, ca. 200 m to the west of the measured section and laterally change into fluvial-alluvial deposits eastward (Figure 4). Overall, there were periodic shifts between slow sedimentation in a lacustrine/palustrine system and rapid sedimentation in an active alluvial system (Figure 3e). The gradational Chu–Sharpyl Dak transition marks an increase in frequency and thickness of the conglomerate beds, while lacustrine beds became thinner. The overlying Sharpyl Dak conglomerates represent a large series of debris flow deposits in a proximal alluvial fan that progressively filled the basin and shifted the lake margin northward (Figure 3g).

5.1.2 | Ak Terek

The straightforward correlation of the polarity pattern retrieved from the Chu group deposits with the geomagnetic polarity time scale indicates that the Chu group was deposited between 6.3 and 2.8 Ma with an average sedimentation rate of 13 cm.ka^{-1}; there is a short interval with a sedimentation rate of 21 cm.ka^{-1} at ca. 5 Ma (Roud et al., 2021). This age model places the Chu–Sharpyl Dak transition at 2.8 Ma (Figure 5). Our ^{26}Al/^{10}Be isochron burial age for the uppermost Chu is 2.71 ± 0.37 Ma (sample AKT-U, Figure 8c; see Figure 5 and Figure S1 for position

of the sample), consistent with the magnetostratigraphic age constraints. The sample from the Sharpyl Dak deposits did not yield reliable results (sample AKT-Q, Figure 8b). However, these two dating methods provide highly consistent results; thus, we can conclude that the Ak Terek section was deposited during the late Miocene–Pliocene.

The Ak Terek section is interpreted to represent the deposits of a meandering river system. The rounded and well-sorted conglomerates and sandstones are mostly granitic and originate from the granites of the Terskey range, as indicated by the predominantly northeast paleocurrent flow directions. The conglomerates were deposited in large channels; together with well-sorted grey sandstones, they comprise the river bed load (Figure 6a). Sandy siltstones and massive mudstones represent a floodplain with episodical fluvial input during flood stages. Repeated alternations between fluvial and floodplain deposits suggest a distal fluvial system with a migrating channel on a floodplain. Pedogenesis occurred in fine-grained deposits throughout the section with thin, immature, rare horizons of small calcrete nodules in the lower part of the section and a gradual upsection increase in their size and abundance (Figure 6b). Calcrete nodule horizons and gypsum layers in the upper part of the section suggest alternation of stronger rainfall and prolonged dry periods (Breecker et al., 2009) with very low sedimentation rates (Alonso-Zarza et al., 1992). The upsection increase in nodule abundance between ca. 6 and 3.5 Ma reflects a Pliocene increase in water availability and seasonality. A decrease in the pedogenic nodule abundance and decreasing thickness of floodplain deposits after ca. 3.5 Ma suggest shortening of periods of slow deposition and soil formation and likely more frequent conglomerate deposition due to an increase in tectonic activity or glaciation in the Terskey range.

5.1.3 | Jergalan

The sequence records a proximal high-energy braided river system gradually transforming into a proximal alluvial fan. Conglomerates in the uppermost parts of the two cliffs represent the fill of a coarse-grained braided river above an angular unconformity (Figure 7b,c). Both channel structures probably represent Quaternary deposition. We interpret the Chu–Sharpyl Dak transition to be represented by the gradational contact between finer and coarser gently dipping deposits; therefore, Sharpyl Dak deposition started when the conglomerates started to prevail. The results from sample JGL17, taken from the bottom of the upper (coarser) part (Figure 7a), suggest that the age of the Chu–Sharpyl Dak transition occurs at 4.26 ± 0.44 Ma (Figure 8h). The stratigraphically

older JGL-2 sample yields an $^{26}Al/^{10}Be$ isochron burial age of 4.76 ± 0.82 Ma when ^{26}Al concentrations are not blank-corrected (Figure 8i2). The above results roughly constrain the Chu–Sharpyl Dak transition in Jergalan to be not older than 5 Ma, that is early Pliocene. This age is notably older than at Kaji Say and Ak Terek, where the transition occurred at 2.8–2.6 Ma. The paleocurrent analysis suggests that the Chu–Sharpyl Dak transition unit was fed by sediments from the Kungey range. Hence, we suggest that exhumation of the eastern Kungey range began at ca. 5 Ma.

5.1.4 | Toru Aygir and Cholpon Ata

The Toru Aygir and Cholpon Ata sequences represent deposits from a meandering fluvial system. A series of channels in the Toru Aygir section with subrounded conglomerates and well-sorted sandstones represent deposition in a high-energy flow from the bedload of a river (Figure 6c). In the Cholpon Ata section, large channels filled with rounded conglomerates and sandstones are interbedded with siltstones and represent the coarse bedload of a migrating channel on a floodplain (Figure 6d). A detailed description of both sections and geological maps of the area is presented in Selander et al. (2012). The Toru Aygir area is also described in details in Bowman et al. (2004).

Both sequences belong to the Chu group. Selander et al. (2012) described two members of the Chu group on the southern flank of the Kungey range—the stratigraphically older Terskey member with northward-flowing paleocurrent indicators, sourced from the Terskey range, and the stratigraphically younger Kungey member with southward-flowing indicators, sourced from the Kungey range. The Terskey member is mapped throughout the range front, while the Kungey member is exposed only in the eastern part of the Kungey range (Figure S2). The initiation of Kungey range growth is estimated to be between 7 and 4 Ma (Selander et al., 2012). The Toru Aygir section is located in the western Kungey range and the Chu deposits there belong to the Terskey member (Figure S2), although our measurements of mainly southward paleocurrent directions contradict data from Selander et al. (2012) (Figure 1c and Figure S3). The Cholpon Ata section is situated in the eastern Kungey range and exhibits both members (Figure S2), although our measurements of mostly southward paleocurrent directions in both the stratigraphically older (Terskey member) and stratigraphically younger (Kungey member) parts of the section also contradict data from Selander et al. (2012) (Figure 1c and Figure S4). This suggests that the Terskey member of the Cholpon Ata and Toru Aygir sections includes deposits

sourced mainly from the Kungey range, in contrast with data from Selander et al. (2012), which show a distinctive prevalence of northward-directed paleocurrents in the Terskey member.

5.2 | Diagenetic characteristics

5.2.1 | Thin-section inspection

Sparitic and poikilotopic calcite cement and mechanical compaction in fluvial-alluvial sandstone samples (Figure 9a,b) suggest that the Ak Terek section and the lower Chu unit of Kaji Say underwent early stages of diagenesis (Worden et al., 2018). Higher temperatures associated with diagenesis may lead to crystal growth within the calcite cements (Worden & Burley, 2003). Therefore, the Ak Terek section and the lower Chu unit of Kaji Say might have undergone a higher degree of recrystallization than sandstones from the beach facies, alluvial and lacustrine deposits with microsparitic cement and micrite of the upper Chu unit of the Kaji Say section (Figure 9c). Nevertheless, some of the samples with poikilotopic cement only have point contacts between grains, which may mean that cementation occurred at an early stage of alteration without substantial burial and compaction. Lacustrine carbonate of the upper Chu unit of the Kaji Say section consists of primary micrite and microsparite and exhibits evidence of palustrine alteration during dry periods without significant burial, such as desiccation cracks and pores with alveolar textures and pore-filling sparitic calcite cement (Figure 9d,e; Alonso-Zarza & Wright, 2010). Microsparite infills porosity in primary lacustrine micrite and can result from primary cementation in a subaerial environment or during pedogenesis (Freytet & Verrecchia, 2002).

5.2.2 | Evaluation of the diagenetic overprint in the stable isotopic record

$\delta^{18}O$ values of carbonate depend on the $\delta^{18}O$ values of the fluid from which carbonate precipitated and on the carbonate formation temperature. As such, carbonate formation and recrystallization under elevated temperatures, as well as the presence of basinal fluids during burial diagenesis, can affect the primary $\delta^{18}O$ values of authigenic carbonate minerals. Higher temperature resetting of $\delta^{18}O$ values during burial and diagenesis typically results in low $\delta^{18}O$ values (e.g. Methner et al., 2016; Quade et al., 2020) due to the temperature dependance of water-calcite fractionation (e.g. Swart, 2015 and references therein). The $\delta^{18}O$ values of the Kaji Say and Ak Terek sections do not yield suspiciously

low $\delta^{18}O$ values that would be associated with deep (higher temperature) burial diagenesis. One could hypothesize that the increasing $\delta^{18}O$ and $\delta^{13}C$ values with stratigraphy in the Kaji Say section could be burial related, that is lower values at the base of the section might reflect a higher level of diagenetic overprint due to higher temperatures. Unlike the Kaji Say samples, those from Ak Terek do not show such a trend; however, the data scatter along the Ak Terek record could reflect alteration in connection with dissolution and reprecipitation of calcite at different temperatures related to different burial depths (Sanyal et al., 2005). Distinctively more positive $\delta^{13}C$ values of lacustrine calcareous mudstone samples suggest that the primary lacustrine isotopic signal was not significantly affected by diagenetic and pedogenetic alteration (Alonso-Zarza, 2003).

We suggest that cementation and pedogenetic alteration happened under similar near-surface meteoric conditions, and we argue that the similarity of $\delta^{18}O$ and $\delta^{13}C$ values of sandstone cement, pedogenic and lacustrine carbonates in the Kaji Say section suggests similar post-depositional environments in the stratigraphically older and younger parts of the Kaji Say section. At the same time, as the values in the Kaji Say and Ak Terek sections overlap (Figure 10), we conclude that the rocks of the Ak Terek and Kaji Say sections reflect similar post-depositional conditions of early diagenesis. Early diagenesis corresponds to near-surface and shallow burial conditions under the influence of the depositional environment when sediments are buried to <2 km and temperatures below 70°C (Worden & Burley, 2003). Early diagenesis does not alter oxygen isotopic values when occurring at near-surface temperatures (Garzione et al., 2004; Sanyal et al., 2005), such as would be expected in the relatively thin stratigraphic sequences that we have studied. Moreover, our stable isotope values overlap with the values from other northern Central Asian sections (Figure 11), the rocks of which were reported to be unaffected by burial diagenesis. As the sedimentary sequences in Central Asia have different thicknesses but
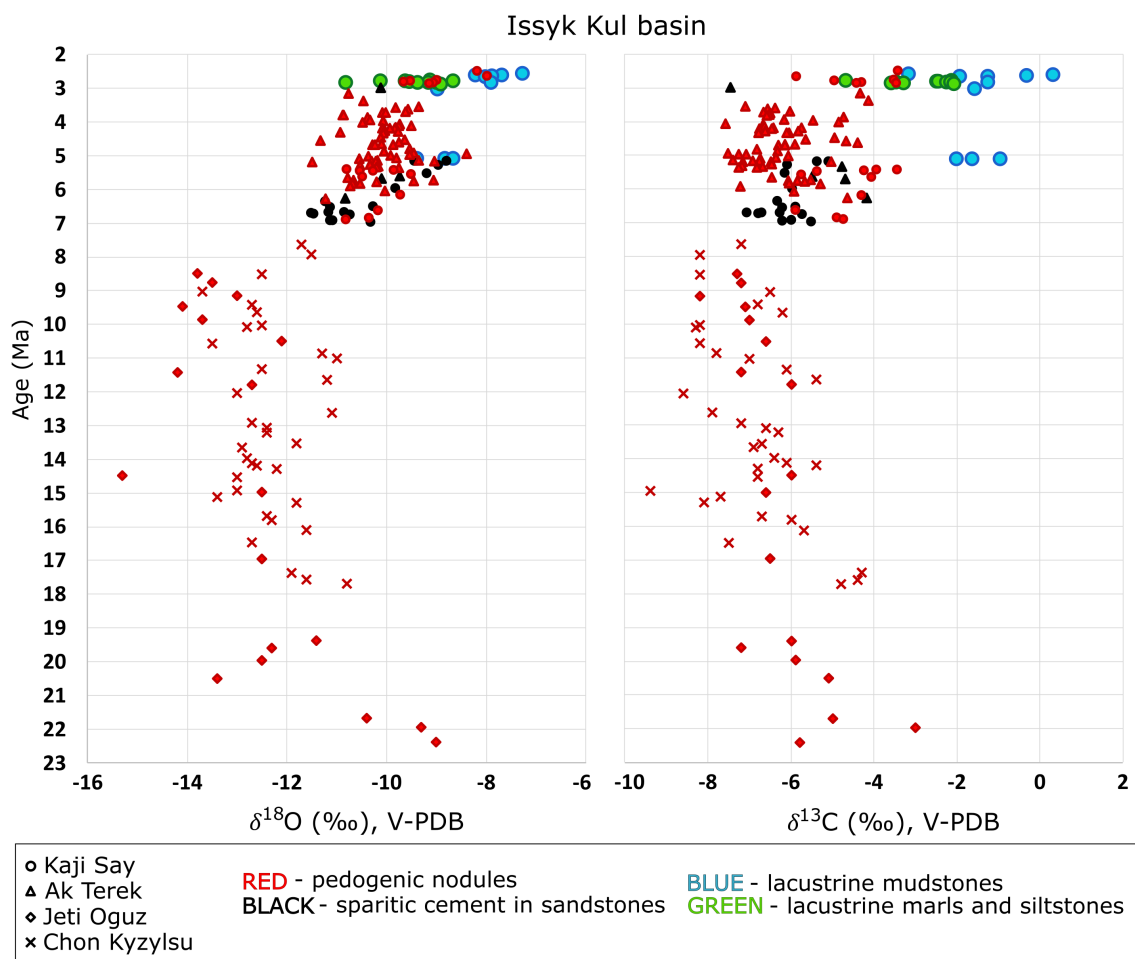
FIGURE 10 $\delta^{18}O$ and $\delta^{13}C$ data from the Issyk-Kul basin plotted against the age model. Kaji Say and Ak Terek data plotted against the original age model of Roud et al. (2021). Using the revised age for the hiatus proposed in this manuscript would shift the lacustrine mudstones plotted at 5 Ma to 3 Ma. Jeti Oguz and Chon Kyzylsu data are from Macaulay et al. (2016), replotted using the age model of Roud et al. (2021).
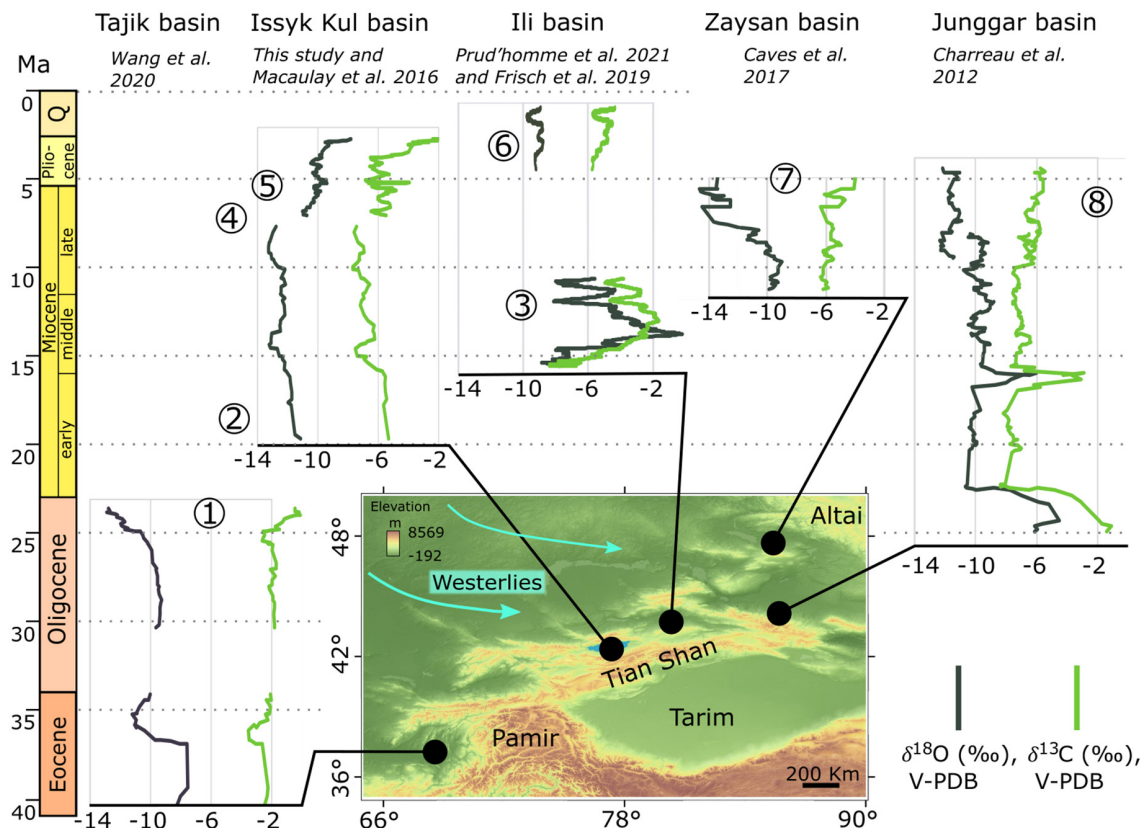
FIGURE 11 New and published δ18O and δ13C data from the basins on the northern (windward) side of the Tian Shan, Altai and Pamir, plotted against age. New data from the Issyk-Kul basin plotted against the original age model of Roud et al. (2021). All data except Ili basin are smoothed using a 6-point moving mean, data from the Ili basin are smoothed using a 30-point moving mean. Ili basin data from Hellwig et al. (2018) are not included due to a lack of age constraints. 1–8 show main events, reflected in the stable isotopic records (interpretations are taken from the corresponding articles): (1–2) windward positions of the Tajik (Wang et al., 2020) and Issyk-Kul (this study and Macaulay et al., 2016) basins due to growing Tian Shan and Pamir; (3) global climatic changes in the Ili basin caused by orbital forcing (Frisch, Voigt, Verestek, et al., 2019), which are not reflected in time-equivalent records from other basins; (4) change from a windward to leeward position of the Issyk-Kul basin due to northward growth of Tian Shan (this study); (5) aridification in the Issyk-Kul basin after Kyrgyz, Kungey and Trans Ili ranges blocked the westerly moisture from reaching the basin (this study); (6) aridification in Central Asia, caused by interactions between the westerlies and the Siberian High (Prud'homme et al., 2021); (7) windward position of the Zaysan basin due to growing Altai (Caves et al., 2017); (8) two records from the Junggar basin are controlled by hypsometry of the drainage basins and do not reflect climatic or tectonic changes (Charreau et al., 2012).

show similar δ18O and δ13C values, burial diagenesis does not appear to have played a major role (Caves Rugenstein & Chamberlain, 2018). We therefore conclude that our sections did not experience late diagenesis and that our isotopic results reflect primary values.

5.3 | Stable isotope analysis

5.3.1 | Stable isotope-based paleoenvironmental reconstructions from continental carbonates

δ18O and δ13C values of terrestrial carbonates may record information on paleoclimate, paleoaltimetry, vegetation types, lake water characteristics and diagenesis,

provided that carbonate precipitation occurs in equilibrium with soil or lake water (e.g. Cerling, 1984; Cerling et al., 1997; Garzione et al., 2004; Levin et al., 2006; Poage & Chamberlain, 2001; Quade et al., 2011; Talbot, 1990).

δ18O values of pedogenic and lacustrine/palustrine carbonate reflect the temperature of carbonate formation and the δ18O values of soil water or lake water, respectively. In the absence of reconstructed carbonate formation temperatures, we interpret the pedogenic carbonate δ18O values in terms of changes in δ18O values of local precipitation (Cerling & Quade, 1993). We interpret the lacustrine and palustrine carbonate δ18O values to reflect average precipitation δ18O values within the catchment area (Talbot, 1990). δ18O may be modified by the impact of lake level and evaporation dynamics. For example, the preferential release of 16O from lake water during

evaporation leads to increased $\delta^{18}O$ values in response to enhanced evaporation.

Mountain growth leads to orographically induced rainout, which preferentially removes ^{18}O from water vapour and results in a systematic decrease in $\delta^{18}O$ values with elevation on the windward side and low $\delta^{18}O$ values in the lee (e.g. Chamberlain et al., 2012; Chamberlain & Poage, 2000; Mulch, 2016; Quade et al., 2011; Rowley & Garzione, 2007). Therefore, $\delta^{18}O$ values of pedogenic and lacustrine carbonates may provide a proxy for the $\delta^{18}O$ of meteoric water and thus paleoelevation of carbonate formation.

Moreover, an increase in pedogenic carbonate $\delta^{18}O$ can point to increased evaporation or a shift in seasonality of precipitation to a warmer season. Aridity of Central Asia leads to an increase in soil and lake water evaporation, resulting in moisture recycling and high and relatively steady $\delta^{18}O$ values (Caves Rugenstein & Chamberlain, 2018). Furthermore, topographic growth of the Tian Shan created a seasonality pattern of winter–spring precipitation on the windward (northwestern) side and summer precipitation within the range and on the leeward (southeastern) side (Baldwin & Vecchi, 2016). Dry winter conditions due to weak westerlies and a dominant Siberian High lead to orographic rainout of the westerly moisture on the windward side in winter, but prevalence of cyclonic activity at high elevations in the summer leads to rainfall at high elevations (Bershaw & Lechler, 2019). This effect results in low $\delta^{18}O$ values of winter precipitation on the windward side and high and steady $\delta^{18}O$ values of summer precipitation within the range and in the lee (Bershaw & Lechler, 2019; Wang et al., 2016).

The $\delta^{13}C$ values of pedogenic carbonates are primarily driven by the carbon isotopic composition of vegetation and ultimately reflect the relative importance of atmospheric and soil-respired CO_2 during their formation (Cerling, 1984; Cerling & Quade, 1993). Reduced precipitation theoretically leads to lower soil respiration rates and subsequently to a decrease in the soil carbonate formation depth and a higher contribution of atmospheric CO_2. Overall, a decrease in precipitation therefore typically results in more positive $\delta^{13}C$ values of pedogenic carbonates (e.g. Caves et al., 2016). Differences in fractionation of $\delta^{13}C$ in C_3 and C_4 plants during photosynthesis lead to ca. 14 per mil lower $\delta^{13}C$ values in C_3 plants. However, we neglect this effect because of scarce abundance of C_4 vegetation in Central Asia (e.g. Caves Rugenstein & Chamberlain, 2018).

Variations in lake carbonate $\delta^{13}C$ values generally reflect changes in biogenic productivity (e.g. Li & Ku, 1997). Because organic matter preferentially takes up the light carbon isotope (^{12}C), increased biogenic productivity leads to a relative increase in ^{13}C in dissolved CO$_2$, which is incorporated in carbonate during precipitation. Therefore, increased biogenic productivity in a lake leads to an increase in $\delta^{13}C$ in lacustrine carbonate. Hydrologically closed basins have no surface outlet, and hence, most water exits the basin through evaporation. $\delta^{13}C$ and $\delta^{18}O$ generally display a covariance in closed basins. This is typically the result of temperature changes during carbonate formation, which governs biogenic productivity as well as evaporation (e.g. Li & Ku, 1997).

5.3.2 | Published stable isotopic records from the windward basins of the Tian Shan and Altai

By combining new stable isotope data from the Kaji Say and Ak Terek sections and published data from the Jeti Oguz and Chon Kyzylsu sections (Macaulay et al., 2016) with the age models for the four sections (Roud et al., 2021), we have compiled a continuous oxygen and carbon stable isotopic record that covers the time interval from the early Miocene to the early Pleistocene (Figure 10).

Other studied windward basins in the Tian Shan and Altai include the Ili basin (Frisch, Voigt, Verestek, et al., 2019; Hellwig et al., 2018; Prud'homme et al., 2021), Tajik basin (Wang et al., 2020), Junggar basin (Charreau et al., 2012) and Zaysan basin (Caves et al., 2017) (Figure 11). In the sedimentary section in the Tajik basin (1800-m-thick, 41–23.3 Ma), mudstones and carbonate cement in sandstones were analysed. The $\delta^{18}O$ record shows a change towards wetter conditions after ca. 25 Ma when the basin setting shifted to a windward position due to the establishment of the Pamir and Tian Shan orographic barrier (Wang et al., 2020). The Kendyrlisai Valley section in the Ili basin is ca. 166-m-thick and is of late Oligocene to early Miocene ages. Starting from ca. 23.3 Ma, the sedimentary sequence records the establishment of a fluvial system, while the $\delta^{18}O$ and $\delta^{13}C$ values of pedogenic carbonates increase and reflect increasing aridity and pronounced seasonality (Hellwig et al., 2018). The Aktau section in the Ili basin (371-m-thick, 15.6–10.6 Ma) provides a sedimentary record with pedogenic and lacustrine carbonates with features of early diagenesis and shows an overall increase in water availability, whereas the $\delta^{18}O$ and $\delta^{13}C$ values reflect changes in the depositional environment due to global climatic changes caused by orbital forcing (Frisch, Voigt, Verestek, et al., 2019). The $\delta^{18}O$ and $\delta^{13}C$ values of sampled pedogenic carbonates of the Charyn Canyon section in the Ili basin (ca. 80-m-thick, 4.5–0.5 Ma) reflect long-term aridification in Central Asia, caused by the interplay between the westerlies and the Siberian High (Prud'homme et al., 2021). In the Kuitun

He (1800 m, ca. 10–4.5 Ma) and Jingou He (4500 m, ca. 26–8 Ma) sections in the Junggar basin, lacustrine and palaeosol carbonates were analysed, as well as carbonate cement from fluvial deposits. The $\delta^{18}O$ values of the two records are interpreted to be controlled by hypsometry of the drainage basin (Charreau et al., 2012). In the Zaysan basin section (188 m, 11.5–5 Ma), pedogenic carbonates were sampled and the late Miocene decrease in $\delta^{18}O$ values is interpreted to reflect the establishment of the spring and fall precipitation due to the downwind topographic growth of the Altai (Caves et al., 2017).

5.3.3 | Climatic conditions from 23 to 8 Ma

$\delta^{18}O$ and $\delta^{13}C$ records from the Jeti Oguz and Chon Kyzylsu sections suggest rather stable long-term climatic conditions between 23 and 8 Ma. One may observe a subtle negative trend upsection from ca. −3 to −5‰ to ca. −7 to −8‰ in $\delta^{13}C$ values and from ca. −9 to −11‰ to ca. −12 to −14‰ in $\delta^{18}O$ values (Figure 10), which may reflect the establishment of windward conditions at higher elevations within the basin and a progressively higher degree of orographic rainout since the early Miocene due to topographic growth of the Terskey range downwind (Figure 12a). The sampled rocks in the Jeti Oguz and Chon Kyzylsu sections are thin overbank deposits with a weak pedogenic overprint; therefore, river run-off water delivered to the river overbank during floodings possibly may have had an impact on stable isotopic values. An increase in catchment area's elevation would cause delivery of water from higher elevations within the Terskey range with lower $\delta^{18}O$ values that would result in lower $\delta^{18}O$ values of the carbonates. Concurrently, wetter conditions would increase soil respiration rates and/or decrease hydraulic stress on the C_3 vegetation and lower $\delta^{13}C$ values (Macaulay et al., 2016). Therefore, this suggests that topographic growth of the Terskey range played the primary role in the decrease of $\delta^{18}O$ and $\delta^{13}C$ values between 23 and 8 Ma.

A similar subtle decreasing trend in $\delta^{18}O$ values from the Tajik basin between ca. 25 and 23.3 Ma suggests the primary role of the growing topography in both Tajik and Issyk-Kul basins (Figure 11). At the same time, the late Oligocene–early Miocene stable isotopic records from the Ili basin show increasing trends of $\delta^{18}O$ from ca. −11 to −7‰ and $\delta^{13}C$ from ca. −9 to −5‰ (Hellwig et al., 2018; these data are not included in Figure 10 due to a lack of age constraints). The time-equivalent part of the Junggar basin $\delta^{18}O$ and $\delta^{13}C$ records shows no trend with $\delta^{18}O$ values of ca. −10‰ and $\delta^{13}C$ values of ca. −8‰ (Figure 11). Not only the $\delta^{18}O$ values but also the $\delta^{13}C$ values from the Issyk-Kul and Ili basins show opposing trends. Whereas

the Issyk-Kul stable isotopic values reflect the topographic growth of the Terskey range, the results from the Ili basin are interpreted to reflect increased evaporation and aridification in Central Asia (Hellwig et al., 2018), and the Junggar record reflects the hypsometry of the drainage basin (Charreau et al., 2012). Even though higher water availability was detected in the Ili basin by the establishment of a fluvial system at ca. 23 Ma (Hellwig et al., 2018), and in the Junggar basin by the presence of lacustrine deposits in the late Oligocene (Charreau et al., 2012), the stable isotopic records from these two basins do not unequivocally point to locally wetter conditions. The slight negative $\delta^{18}O$ and $\delta^{13}C$ trends in the early Miocene deposits of the Issyk-Kul basin suggest wetter conditions that are mainly controlled by local topographic, rather than regional or global climatic factors.

The middle Miocene Issyk-Kul and Ili stable isotope records show drastically different values and trends (Figure 11). This can be explained by the difference in data resolution and the sampled sediment facies. The Ili basin represents lacustrine and distal alluvial facies and has 821 measurements spread over ca. 5 Ma (371 m; Frisch, Voigt, Verestek, et al., 2019), whereas the Jeti Oguz and Chon Kyzylsu records include 53 samples, which were taken from overbank pedogenic horizons and spread over ca. 15 Ma. The low-resolution Issyk-Kul record of isotopic values obtained from pedogenic carbonate is therefore mostly driven by long-term climatic conditions. By contrast, the Ili sedimentary succession reflects global climatic and orbital changes (Frisch, Voigt, Voigt, et al., 2019; Voigt et al., 2017), and the Ili stable isotopic record is reported to be primarily controlled by the changes in the depositional environment (Frisch, Voigt, Verestek, et al., 2019). Therefore, these two records cannot be directly compared. The Issyk-Kul, Zaysan and Junggar stable isotopic records of pedogenic carbonates suggest comparable and relatively unchanged paleoenvironments up to ca. 8 Ma with no significant influence of either climatic changes or mountain growth in the middle Miocene (Figure 11).

5.3.4 | Positive shift in $\delta^{18}O$ and $\delta^{13}C$ values between 8 and 7 Ma

Between 8 and 7 Ma, we observe a distinctive ca. 2‰ positive shift of $\delta^{18}O$ and $\delta^{13}C$ values within the Issyk-Kul basin (Figure 10). The shift occurs during a ca. 0.6 Ma gap in the combined Issyk-Kul basin record and occurs between the records from the Jeti Oguz and Chon Kyzylsu sections and the records from the Kaji Say and Ak Terek sections.

There are several possible mechanisms that could induce a ca. 2‰ shift in $\delta^{18}O$ and $\delta^{13}C$ values at 8–7 Ma. (1) Given that the ca. 0.6 Ma stratigraphic gap coincides with
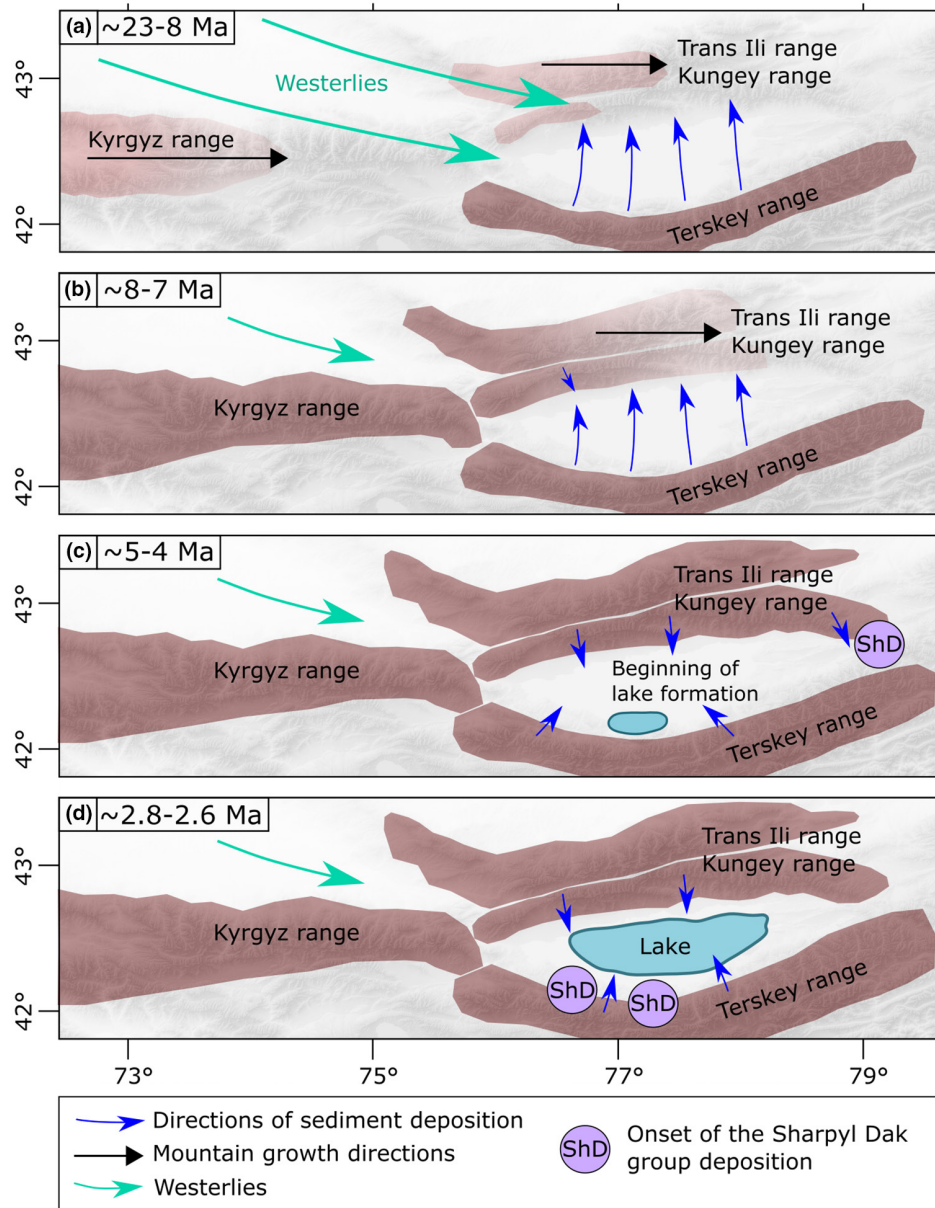
FIGURE 12 Schematic representation depicting the Neogene development of the Issyk-Kul basin. (a) Windward position of the Issyk-Kul basin due to growing Terskey range. Sediments from the Terskey range reach the low-elevated Kungey range area. (b) Sufficient surface uplift of the Kyrgyz, Kungey and Trans Ili ranges prevent the westerlies from reaching the Issyk-Kul basin. Issyk-Kul basin became leeward. (c) Beginning of lake formation in the Kaji Say area and commencement of Sharpyl Dak deposition in Jergalan due to tectonic activity. Sharpyl Dak sediments in Jergalan are sourced from the Kungey range. (d) Lake expansion and commencement of Sharpyl Dak deposition in the Kaji Say and Ak Terek areas.

a change in sampling localities, the decrease in $\delta^{18}O$ values may result from spatial environmental changes within the basin (Figure 1c). (2) An orographically induced change from a windward to a leeward position of the basin by changes in atmospheric circulation and topography to the northwest, blocking of moisture-bearing westerlies, and an increase in evaporation and aridification. (3) Global cooling and retreat of the Paratethys, the proximal moisture source for Central Asia, to the west, which reduced the amount of water vapour in the atmosphere and

enhanced aridification during Miocene times (e.g. Miao et al., 2012; Ramstein et al., 1997; Zachos et al., 2001).

Differences in the geographic positions and depositional environments between the sections within the Issyk-Kul basin likely did not play a role in creating the observed change in $\delta^{18}O$ and $\delta^{13}C$ values. The amount of moisture and precipitation and the isotopic composition of rainfall and mean annual temperature were likely the same within the basin. Even though the Kaji Say section is situated ca. 70 km west from the Jeti Oguz and Chon Kyzylsu

sections, it is also ca. 50 km east from the Ak Terek section, and the δ¹⁸O and δ¹³C values at Kaji Say and Ak Terek overlap. Also, the Jeti Oguz and Chon Kyzylsu sections belong to the Shamsi sedimentary group, which consists of coarser-grained deposits than the Chu group of the Kaji Say and Ak Terek sections. However, there was no isotopic shift or change of trend in the coarse-grained alluvial deposits of the upper Chu and Sharpyl Dak groups compared with the finer-grained lower Chu deposits in the Kaji Say section. The match of the timing of the Shamsi–Chu transition and the shift in stable isotopic values mark a significant tectonic event that could have reorganized local climate and fluvial systems. We consider the intensification of basin-wide evaporation and aridification through changes in topography as the most plausible explanation for this observed shift. Contemporaneous stable isotope data from the Zaysan (Caves et al., 2017) and Junggar (Charreau et al., 2012) basins do not show a similar shift in δ¹⁸O and δ¹³C values or changes in the trends in the late Miocene (Figure 11). Therefore, we conclude that the positive shift had a local, rather than a regional or global driver, and that global cooling and Paratethys retreat were unlikely to have caused the isotopic shift in the Issyk-Kul record.

Low-temperature thermochronological data show that the onset of deformation in the Terskey, Trans Ili and Kungey ranges occurred during the late Oligocene–early Miocene (De Grave et al., 2013; De Pelsmaeker et al., 2015; Macaulay et al., 2013, 2014), with a second pulse of exhumation during the middle-late Miocene (Macaulay et al., 2014). Paleocurrent data from the Kungey range (Selander et al., 2012) indicate that sediments from the southerly Terskey range were deposited in the Kungey area during the middle Miocene, implying that the Kungey range was relatively low-lying at that time; thus, Selander et al. (2012) proposed that substantial uplift of the Kungey happened during the second pulse of exhumation between 7 and 4 Ma. Thermochronological data from the Kyrgyz range, northwest of the Issyk-Kul basin, indicate that range uplift prograded eastward from 11 to 7 Ma (Bullen et al., 2001, 2003; Sobel, Oskin, et al., 2006).

We therefore interpret the ca. 2‰ shift in δ¹⁸O and δ¹³C values between 8 and 7 Ma to be caused by sufficient surface uplift (ca. 1300–2000 m, Bookhagen & Burbank, 2010; Bookhagen & Strecker, 2008) of the Kyrgyz range, as well as the growth of the Trans Ili and Kungey ranges. The isotopic shift therefore reflects a change from a more windward to a more leeward position of the Issyk-Kul basin (Figure 12a,b). Prior to surface uplift of the aforementioned ranges, the Issyk-Kul basin received moisture by the westerlies coming mainly from the NW. The formation of a rain shadow would lead to a decrease in δ¹⁸O values in the basin due to orographically induced rainout on the windward sides of the Kyrgyz, Trans Ili and Kungey

ranges. However, the ca. 2‰ shift and the switch of the stable isotopic trend from increasingly negative values between ca. 23 and 8 Ma to increasingly positive δ¹⁸O values and relatively steady δ¹³C values rather reflect an increase in aridity and evaporation as a result of surface uplift after ca. 8–7 Ma. Moreover, the change from a windward to a leeward position might have caused a change in the seasonality of precipitation due to interactions of the moisture-bearing air masses with high topography. At present, the Issyk-Kul basin is characterized by a spring and summer precipitation regime with higher δ¹⁸O values of summer precipitation than winter precipitation (Baldwin & Vecchi, 2016; Macaulay et al., 2016; Wang et al., 2016). We suggest that the simultaneous establishment of a rain shadow, which would lower the δ¹⁸O values, and an associated increase in aridity and change in the seasonality of precipitation, which would lead to an increase in the δ¹⁸O values, led to a combined ca. 2‰ positive shift in the δ¹⁸O record.

5.3.5 | Climatic conditions from 7 to 2.5 Ma

Between 7 and 5 Ma, a subtle upsection trend towards more positive δ¹⁸O and δ¹³C values can be observed in Kaji Say. In Ak Terek, δ¹⁸O and δ¹³C values are more variable and lack a trend, which can reflect natural scatter of isotopic values and indicate a steady fluvial environment with no noticeable climatic changes. A meandering river, situated farther from the range front, has more diverse water sources and a larger drainage area than a proximal braided river near the range front. This results in the accumulation of run-off water with variable isotopic signals on a floodplain and, subsequently, in higher variability of δ¹⁸O values in the water of a meandering rather than a braided river (Kent-Corson et al., 2009). Sediments in the two studied sections primarily record the isotopic signal of run-off river water, because, as mentioned previously, in the Issyk-Kul basin summer rainout occurs at high elevations (Bershaw & Lechler, 2019), which is supported by palynology (Fortuna, 2016). Therefore, between 7 and 5 Ma, the difference in Kaji Say and Ak Terek stable isotopic records may reflect a small difference between a more proximal position with respect to the Terskey range front of a braided river in Kaji Say and a more distal position of a meandering river at Ak Terek. The proximal position of the Kaji Say section with a smaller drainage area could result in higher sensitivity of pedogenic carbonates to changes in water isotopic composition and lead to the creation of the observed trend. Nevertheless, between 6.3 and 5 Ma, the δ¹⁸O and δ¹³C values from the two sections overlap, suggesting a similar fluvial environment across the basin.

In the lower Chu unit of the Kaji Say section (fluvial-alluvial, 0–450 m; Figure 2), $\delta^{18}O$ and $\delta^{13}C$ values of sandstone cement and pedogenic carbonates are comparable (average values: $\delta^{18}O_{cement} = -10.4 \pm 0.9‰$ and $\delta^{18}O_{pedogenic} = -10.2 \pm 0.4‰$; $\delta^{13}C_{cement} = -6.1 \pm 0.5‰$ and $\delta^{13}C_{pedogenic} = -4.7 \pm 0.8‰$), suggesting that both types of carbonate formed in similar near-surface conditions from meteoric water. In the upper Chu and the Sharpyl Dak units (alluvial and lacustrine, 450–700 m; Figure 2), lacustrine $\delta^{18}O$ values are comparable to the pedogenic carbonate $\delta^{18}O$ values and sustain the trend towards more positive values without abrupt changes (average values: $\delta^{18}O_{lacustrine} = -8.8 \pm 0.9‰$ and $\delta^{18}O_{pedogenic} = -8.9 \pm 0.6‰$). This suggests that pedogenic and lacustrine carbonates reflect similar conditions and that the lake did not experience significant evaporation, which would increase the $\delta^{18}O$ and $\delta^{13}C$ values. The lacustrine samples from the Kaji Say section show a relatively weak correlation between the $\delta^{18}O$ and $\delta^{13}C$ values, with $r = 0.49$. Poor correlation with $r < 0.7$ (Talbot, 1990) suggests a hydrologically open lake system with relatively short water residence time and $\delta^{18}O$ values reflecting the isotopic composition of rainfall and inflowing river water (Leng & Marshall, 2004; Talbot, 1990). By contrast, the isotopic composition of lacustrine carbonates in closed lakes is mainly controlled by the hydrological balance and evaporation, so that the $\delta^{18}O$ and $\delta^{13}C$ values of lake water reflect lake-level changes, showing variable and high $\delta^{18}O$ values and a strong covariance between $\delta^{18}O$ and $\delta^{13}C$ (Leng & Marshall, 2004; Li & Ku, 1997). The upper Chu and Sharpyl Dak units have more positive lacustrine mudstone $\delta^{13}C$ values (average value: $\delta^{13}C_{lacustrine\ mudstone} = -1.4 \pm 1.0‰$), while lacustrine marls and siltstones samples yield $\delta^{13}C$ values between those from pedogenic carbonates and lacustrine mudstones (average values: $\delta^{13}C_{lacustrine\ marl\ and\ siltstone} = -2.9 \pm 0.9‰$ and $\delta^{13}C_{pedogenic} = -4.3 \pm 0.9‰$). The distinctively more positive lacustrine mudstone $\delta^{13}C$ values likely represent higher biogenic activity within the lake.

Between 7 and 5 Ma, a subtle trend towards positive $\delta^{18}O$ values can be observed in the combined Issyk-Kul record when the data from the Kaji Say and Ak Terek sections are merged (Figure 10). This is in agreement with gradual aridification in the basin, which was primarily caused by the growth of the Kyrgyz, Kungey and Trans Ili ranges upwind and was also suggested by the spore and pollen data (Grigina & Fortuna, 1981). Aridification across Central Asia was enhanced since ca. 8–7 Ma (Jia et al., 2020), and global cooling intensified between ca. 7 and 5.4 Ma (Herbert et al., 2016). Therefore, primarily orographically induced aridification in the Issyk-Kul basin might have been sustained and amplified by global factors. During this period, the $\delta^{18}O$ and $\delta^{13}C$ data are comparable

in the Issyk-Kul and Junggar basins and reflect similar climatic conditions (Figure 11). The ca. 2‰ difference in $\delta^{18}O$ values of the two records from the Junggar basin is interpreted to be caused by differences in elevation of the catchment area (Charreau et al., 2012), which might also be the case for the ca. 2‰ difference between the Issyk-Kul and Junggar records. The ca. 4‰ lower $\delta^{18}O$ values from the Zaysan basin compared with Issyk-Kul can be explained by the windward position of the Zaysan basin, while the Issyk-Kul basin maintained a leeward position starting from ca. 8 Ma (Figure 11). Growth of the Altai, downwind from the Zaysan basin, led to changes in the interactions of the cyclones and topography, and, subsequently, in the seasonality of precipitation, resulting in a decrease in $\delta^{18}O$ values (Caves et al., 2017).

From 4.5 to 2.5 Ma, the stable isotopic values from the Issyk-Kul basin are comparable to the values from the nearby Ili basin (Figure 11). The Ili basin record is interpreted to be primarily controlled by global climatic changes and to reflect relatively warm and wet conditions between ca. 4.5 and 3.3 Ma with the dominance of the westerlies and aridification between ca. 3.3 and 2 Ma due to a southward shift of the westerlies and the prevalence of dry air masses from the Siberian High (Prud'homme et al., 2021). The similarity in records from the two basins indicates that the primarily orographically induced aridification in the Issyk-Kul basin has been enhanced by these changes in the moisture source at that time.

We conclude that the stable isotopic record from the Issyk-Kul basin reflects a relatively steady environment of a leeward basin with a possible influence of global climatic changes from ca. 7 to 2 Ma. Similarity in records from the northern side of the Tian Shan (Issyk-Kul, Ili, and Junggar basins) may indicate that during this time the character of interactions between the Tian Shan and the westerlies was relatively steady and similar along the range.

5.4 | Pliocene hiatus and lake formation in the Kaji Say area

5.4.1 | Three episodes of deformation

Deciphering the relative importance of climate and tectonics on the creation of lake Issyk-Kul requires understanding the stratigraphic, climatic and tectonic records of the formation of the Issyk-Kul basin. The most useful record for this purpose comes from the Kaji Say area, where we see evidence of three deformation episodes.

The first deformation episode recorded in the section occurred at about 5 Ma. The braided river system, which delivered grey granitic conglomerates, was succeeded by lacustrine deposition. The decrease in fluvial clastic input

allowed time for lacustrine carbonate mud to precipitate during periods of lake highstands and for pedogenic carbonate to form during dry periods. We suggest that deformation close to the modern Terskey range front was responsible for a change in drainage pattern; clastic material was apparently delivered either to the east or west along strike. Lacustrine deposition with reduced clastic input in a subsiding basin may reflect slower accumulation rates than in a fluvial system. Lacustrine deposition periodically alternated with short and intensive debris flows, which led to the deposition of poorly sorted matrix-supported angular rocks from the Taldysui subvolcanic complex, which is the nearest source area. These pulses could have been caused by either an increase in local tectonic activity, by climatically driven floods, or the combination of the two factors.

Northwestern thickening of the beds in the upper Chu unit indicates the presence of growth strata, which record the second episode of deformation (Figure 4). The growth strata can be observed at ca. 480–640 m in the stratigraphic section (Figure 3f), that is after the 2 Ma hiatus proposed by Roud et al. (2021). There is no visible unconformity at the base or within the growth strata and the bedding strike does not change; therefore, the orientation of the stress field likely did not change at this time.

The third episode of deformation is represented by folding of the section. This fold is very tight to overturned and only affects the stratigraphy between ca. 245–480 m in the stratigraphic section, which is deeper in the section than the growth strata and located on the eastern flank of this outcrop. The core of the fold is marked by vertically dipping strata. However, both the overlying growth strata, observed to the northwest, and the base of the section, observed to the south-southeast, have much gentler dips (Figure 4). We suggest that this stage of deformation is younger than 2 Ma, because there is no unconformity within the section and because this folding would have prevented northward transportation of the coarse Sharpyl Dak sediments, which outcrop on the north side of this fold.

5.4.2 | Lake formation in the late Miocene

Lake formation started in the late Miocene in the southern part of the basin in the Kaji Say area (Figure 12). There, individual lacustrine and beach beds transition into fluvial sandstone beds eastward or grow thinner and disappear. Growth strata also thicken to the west. This suggests that the deeper part of the basin was located westward along strike. The first lacustrine and beach facies deposits observed in the area are stratigraphically older than those recorded in the described Kaji Say section. They appear

ca. 200 m to the west and do not reach the measured section (Figure 4). Their stratigraphic position roughly corresponds to 360–380 m in our studied section. Gradual lake progression and northwest thickening of the growth strata suggest enhanced subsidence to the west of the section during the late Miocene–Pliocene. This generally agrees with shallow seismic reflection data from the lake basin that shows that in Holocene time, subsidence was higher in the southern part of the lake basin than in the northern part (Gebhardt et al., 2017). Eastward growth of the Terskey range in the middle−late Miocene (Macaulay et al., 2014) and eastward spreading of the depositional area due to the growth of the Kungey range in the late Miocene (Selander et al., 2012) support the idea that higher subsidence occurred in the southwestern part of the basin. However, the steady fluvial environment in the Ak Terek section shows that the lake first formed locally in the Kaji Say area. We conclude that enhanced subsidence in the Kaji Say area (and likely farther north, beneath the modern lake) led to the formation of a topographic depression in the late Miocene and enabled the formation of the lake on the southern side of the basin. Enhanced subsidence led most likely simultaneously to an internally drained basin, that is a closed basin without a surface outlet. Therefore, even though moisture delivery was reduced due to the creation of an orographic barrier, moisture retention in the closed basin resulted in a lake phase. Furthermore, sedimentological evidence of a local shallow lake presence in the early Miocene–Pliocene was observed in the subsurface deposits obtained from the boreholes on the eastern side of the basin (Grigina & Fortuna, 1981; Voskresenskaya, 2013; Voskresenskaya & Leflat, 2015). However, this age constraint is based only on lithostratigraphical correlation of the deposits to the Shamsi and Chu groups and therefore is imprecise.

5.4.3 | Position of the hiatus

Roud et al. (2021) proposed a 2 Ma hiatus between ca. 5 and 3 Ma based on the interpretation of the magnetic polarity record (Figure 2). The hiatus may be detected by a short interval of one reversed and two transitional polarity samples within a long normal polarity interval. The hiatus was placed at 475 m in the section within an alternation of thin lacustrine mudstones, marls and sandstones. The end of the hiatus roughly marks the beginning of the growth strata formation. Here, we discuss the hiatus in terms of the sedimentology and the depositional system. The position of the hiatus at 475 m within the interbedded beach and lacustrine deposits might be caused by changes in fluvial input and the disappearance of the braided river system in response to the first stage of deformation

in the area. However, deposition of thin, lacustrine and beach sandstone beds implies rapid changes in the depositional environment, which may not be consistent with a depositional hiatus. Moreover, pedogenic alteration in the lacustrine mudstone is weak, indicating that dry periods with no sedimentation were relatively short (Alonso-Zarza, 2003). We suggest that the hiatus actually occurred slightly earlier, during deposition of the first beach facies at 450 m in the section (a shift from lower Chu to upper Chu; Figure 2). We assume that the presence of the lake might not be recorded in local stratigraphy if the lake margin and beach position did not change significantly over a period of time. Reworking of material to sustain the beach would prevent rapid soil formation. Together with the disappearance of the braided river system, this would create a gap in the stratigraphic record. This 1.5-m-thick beach sandstone bed at 450 m in the section consists of well-reworked and sorted coarse quartz sandstone and is laterally continuous. Such characteristics suggest a long-term and stable beach position without frequent lake transgressions and represent a more plausible stratigraphic location for the hiatus. This interpretation stipulates that the position of the hiatus is within the interval of normal magnetic polarity. Assuming a continuous accumulation rate of ca. 23 cm.ka^{-1}, the 25 m downward shift of the stratigraphic position would correspond to an increase of ca. 100 ka in the age of the hiatus, that is it would place the hiatus between 5.2 and 3.1 Ma rather than between 5.1 and 3.0 Ma.

As mentioned previously, the Kaji Say section consists of the western and eastern transects, situated in different valleys (Figure 4). The reversed and transitional polarity samples, which bound the interpreted hiatus, are situated at the base of the western transect. We cannot exclude the possibility that the lacustrine deposits with slow accumulation rates represent a condensed section and some magnetic reversals might have been missed between the two transects. We note that lacustrine micritic carbonates were avoided while collecting paleomagnetic samples as they would likely provide a biased and unreliable magnetic record (Roud et al., 2021). The hiatus may also be misplaced due to general differences in the sedimentation rates of fluvial-alluvial and lacustrine deposits. As we discussed earlier, lacustrine deposits gradually change into fluvial-alluvial sandstones eastward in the Kaji Say area and, therefore, the sedimentation rates also can change laterally. It may be that instead of one long hiatus, the lake experienced a series of shorter hiatuses because of the shifts between the periods of slow lake sediment accumulation, pedogenesis and rapid debris flow deposition. The studied section may not represent a complete magnetostratigraphic sequence or the polarity intervals may be of different stratigraphic thickness due to increase in sedimentation rates from lacustrine to fluvial environment.

However, variations in alternation of lacustrine and fluvial-alluvial deposits in the Kaji Say area can only affect the distribution of possible hiatus positions in the middle of the section. A fluvial system of the lower part of the section represents a steady depositional environment without changes along strike. Moreover, the robust correlation of the magnetostratigraphic age model and $^{26}Al/^{10}Be$ data proves the 2.8–2.6 Ma age of the Chu–Sharpyl Dak transition. Therefore, we consider the overall magnetostratigraphic model to be reliable.

5.5 | Tectonic and climatic development of the Issyk-Kul basin in the late Miocene–Pliocene

5.5.1 | Diachronous deposition of the Sharpyl Dak group conglomerates

The hiatus in the Kaji Say section at ca. 5 Ma and disappearance of grey granitic conglomerates possibly reflect tectonically driven reorganization of the local river system. Intensified tectonic activity in the early Pliocene is also indicated by a short period of increased sedimentation rates in the Ak Terek section at 5 Ma (Roud et al., 2021), and 4–5 Ma onset of Sharpyl Dak deposition at Jergalan. South-directed paleocurrents at Jergalan suggest that Sharpyl Dak deposits were sourced from the Kungey range. Deposition of the Sharpyl Dak group at Jergalan ca. 2 Ma earlier than in the Kaji Say and Ak Terek sections could be driven tectonically because of the eastward progradation of the Kungey range (Figure 12). Thermochronological data also show that exhumation increased at 15–5 Ma in the Kyrgyz Tian Shan and that the Terskey range also grew eastward, although lateral propagation was complicated as the deformation in the Terskey range progressed out of sequence (Macaulay et al., 2014). The Xiyu group in the Chinese Tian Shan, which is analogous to the Sharpyl Dak group in the Kyrgyz Tian Shan, is reported to be deposited diachronously with the ages from 15 to 0.7 Ma across Central Asia (e.g. Chen et al., 2002; Heermance et al., 2007). Xiyu deposits have a ca. 3 Ma age difference in the Junggar basin (Charreau et al., 2009). In the Junggar basin, the late Miocene Xiyu-like deposits are related to tectonic activity, while deposition of the younger Pliocene-Pleistocene conglomerates is believed to be induced by the onset of the Northern Hemisphere glaciation (Zhao et al., 2021). Therefore, a ca. 2 Ma age difference for the onset of Sharpyl Dak deposition within the Issyk-Kul basin is plausible. Intensive Pliocene conglomerate deposition in the Jergalan area might have temporarily blocked westward-draining rivers, possibly permanently blocking a paleo-drainage connection with the Ketmensk basin,

causing sediment starvation in the Issyk-Kul basin and helping the lake expand. Channels feeding the eastern submerged lake delta are visible now and are associated with the modern rivers that flow westward into the lake (De Batist et al., 2002).

5.5.2 | Influence of global climatic changes on sedimentation and lake development in the basin

The Pliocene was characterized by the meridional poleward shift of the westerlies, responsible for changes in moisture delivery (Abell et al., 2021). This shift of the westerlies at 5–3.3 Ma caused relatively high rainfall and fluvial activity in Northern Central Asia, as detected in the windward Ili basin (Prud'homme et al., 2021). Although our stable isotopic data do not show intensifying influence of the westerlies, the spore and pollen data from the Issyk-Kul basin suggest wetter conditions in the early Pliocene (Grigina & Fortuna, 1981). We suggest that despite the leeward position of the Issyk-Kul basin, a relatively high level of precipitation and water availability might be marked by expansion of a lake in the Kaji Say area and by the presence of a steady meandering river at Ak Terek with increasing abundance of paleosols from ca. 6 to 3.5 Ma. Increased precipitation might also have enhanced tectonically driven sedimentation in the Jergalan area.

Late Pliocene expansion of the Northern Hemisphere ice sheets caused a southward shift of the westerlies (Abell et al., 2021). The Siberian High reached the Tian Shan and amplified aridification in Northern Central Asia (Prud'homme et al., 2021). Cooling, aridification, increased aeolian sedimentation in the Ili basin since ca. 3.3 Ma and increased erosion in the Junggar basin since ca. 3 Ma are interpreted to be triggered by the prevalence of cold and dry air masses of the strengthened Siberian High and connected to the onset of Northern Hemisphere glaciation (Charreau et al., 2011; Prud'homme et al., 2021). In the Tarim basin, southward-shifted westerlies enhanced aridification since ca. 2.7 Ma (Fang et al., 2020), and a possible Northern Hemisphere glaciation impact was detected in the Qaidam basin since ca. 3.3 Ma (Zhuang et al., 2011). In the Issyk-Kul basin, increased sedimentation and continuing aridification might have been enhanced by the Siberian High and Northern Hemisphere glaciation. Accumulation of the alluvial fan debris flow deposits since ca. 3 Ma at Kaji Say, an increase in the abundance of conglomerates at Ak Terek since ca. 3.5 Ma, as well as deposition of the Sharpyl Dak conglomerates at Ak Terek and Kaji Say since ca. 2.7 Ma may reflect the accumulation of sediments derived from upstream glaciation, as well as tectonically driven deposition. The spore and pollen data suggest intensified aridification in the basin in the late Pliocene (Grigina & Fortuna, 1981). Increased evaporation due to aridification and vast conglomerate accumulation have affected the lake-level fluctuations and moved the lake shore from the Kaji Say area towards the centre of the basin (Figure 12d). Lake-level variations of at least 400 m in Issyk-Kul during the Holocene are also connected to changes in precipitation and evaporation due to interactions between the westerlies and the Siberian High rather than tectonic activity (Gebhardt et al., 2017). Today, the Issyk-Kul basin is an underfilled basin, with water depths of up to 668 m. The main sediment input since middle Pleistocene is represented by a westward-propagating delta system at the east end of the lake (De Batist et al., 2002; Gebhardt et al., 2017). We propose that the onset of lacustrine deposition at ca. 5 Ma reflects the commencement of the underfilled basin system. However, proof of this hypothesis will require stratigraphic information taken from deep cores within the lake. A related question is whether basin-wide accumulation rates remained constant but subsidence rates increased or that accumulation rates were drastically reduced.

6 | CONCLUSIONS

The most notable finding of our study of the Issyk-Kul basin is an environmental change that is expressed by a shift of ca. 2‰ in $\delta^{18}O$ and $\delta^{13}C$ values at ca. 8–7 Ma and an associated change from a negative to a positive stable isotopic trend. We suggest that the upwind growth of the Kyrgyz, Kungey and Trans Ili (Zaili) ranges created an orographic barrier that diverted westerly moisture sources at ca. 8–7 Ma, which changed the position of the Issyk-Kul basin from windward to leeward, and led to the establishment of the modern-day spring and summer precipitation regime. The associated creation of a rain shadow led to enhanced aridification and evaporation, as expressed in $\delta^{18}O$ and $\delta^{13}C$ values. During the late Miocene–Pliocene, the primarily orographically induced aridification in the Issyk-Kul basin has likely been strengthened by the periodic dominance of dry air masses of the Siberian High during Northern Hemisphere glaciations, when the moisture-bearing westerlies shifted southward.

The transition from the Chu sedimentary group, which consist of fluvial-alluvial sandstones and conglomerates, to massive alluvial conglomerates of the Sharpyl Dak group marks the change from a fluvial-alluvial system to a proximal alluvial fan. Our $^{26}Al/^{10}Be$ isochron burial data suggest a 5–4 Ma age for the transition between the Chu and Sharpyl Dak sedimentary groups in the eastern part of the basin in the Jergalan area; south-directed paleocurrents there suggest the growth of the eastern Kungey

range at 5–4 Ma. Also, ^{26}Al/^{10}Be isochron burial dating confirms the previously proposed 2.6–2.8 Ma age of the transition between the Chu and Sharpyl Dak sedimentary groups on the southern side of the Issyk-Kul basin (Roud et al., 2021). Initiation of the Sharpyl Dak conglomerates' deposition at 2.6–2.8 Ma on the southern side of the basin could have been induced tectonically or by the North Hemisphere glaciation, while older late Pliocene Sharpyl Dak deposition in the Jergalan area is related to intensified tectonic activity.

We propose the formation of an internally drained lake Issyk-Kul at ca. 5 Ma on the southern side of the basin due to enhanced subsidence and reorganization of the river systems in the Kaji Say area. Initiation of lake formation coincides with the disappearance of the braided river system and a 2 Ma hiatus in deposition. Changes in the fluvial network and basin subsidence rates were likely induced by deformation of the Terskey range. We suggest that the hiatus occurred because of fluctuations of the water level in a shallow lake with dry periods of very slow sedimentation and a stable lake margin, so that the beach facies deposits were regularly reworked without subsequent sediment accumulation or pedogenesis. Aridification and conglomerate accumulation since the late Pliocene have moved the lake shore towards the centre of the basin.

CONFLICT OF INTEREST

No, there is no conflict of interest.

PEER REVIEW

The peer review history for this article is available at https://publons.com/publon/10.1111/bre.12751.

DATA AVAILABILITY STATEMENT

Additional information can be found in the online version.

ORCID

Anna Kudriavtseva https://orcid.org/0000-0002-8710-9919
Edward R. Sobel https://orcid.org/0000-0001-5030-8773
Alexandru T. Codilean https://orcid.org/0000-0003-1895-5633
Maud J. M. Meijers https://orcid.org/0000-0003-2724-4980
Gregory D. Hoke https://orcid.org/0000-0002-3720-3245
Réka-H. Fülöp https://orcid.org/0000-0002-3237-0319
Klaus M. Wilcken https://orcid.org/0000-0002-6870-2047
T. Gabriel Enge https://orcid.org/0000-0001-9381-6495

REFERENCES

Abdrakhmatov, K., Aldazhanov, S., Hager, B., Hamburger, M., Herring, T., Kalabaev, K., Makarov, V., Molnar, P., Panasyuk, S., Prilepin, M., & Reilinger, R. (1996). Relatively recent construction of the Tien Shan inferred from GPS measurements of present-day crustal deformation rates. *Nature*, *384*(6608), 450–453. https://doi.org/10.1038/384450a0

Abdrakhmatov, K., Djanuzakov, K. D., & Delvaux, D. (2002). Active tectonics and seismic hazard of the Issyk-Kul Basin in the Kyrgyz Tian-Shan. In J. Klerkx & B. Imanackunov (Eds.), *Lake Issyk-Kul: Its natural environment*. NATO Science Series, 13. Springer. https://doi.org/10.1007/978-94-010-0491-6_11

Abdrakhmatov, K., Weldon, R., Thompson, S. C., Burbank, D. W., Rubin, C., Miller, M., & Molnar, P. (2001). Onset, style and current rate of shortening in the central Tien Shan, Kyrgyz Republic. *Russian Geology and Geophysics*, *42*(10), 1585–1609.

Abell, J. T., Winckler, G., Anderson, R. F., & Herbert, T. D. (2021). Poleward and weakened westerlies during Pliocene warmth. *Nature*, *589*(7840), 70–75. https://doi.org/10.1038/s41586-020-03062-1

Aizen, E. M., Aizen, V. B., Melack, J. M., Nakamura, T., & Ohta, T. (2001). Precipitation and atmospheric circulation patterns at mid-latitudes of Asia. *International Journal of Climatology: A Journal of the Royal Meteorological Society*, *21*(5), 535–556. https://doi.org/10.1002/joc.626

Aizen, V. B., Aizen, E. M., Joswiak, D. R., Fujita, K., Takeuchi, N., & Nikitin, S. A. (2006). Climatic and atmospheric circulation pattern variability from ice-core isotope/geochemistry records (Altai, Tien Shan and Tibet). *Annals of Glaciology*, *43*, 49–60. https://doi.org/10.3189/172756406781812078

Aizen, V. B., Aizen, E. M., Melack, J. M., & Dozier, J. (1997). Climatic and hydrologic changes in the Tien Shan, Central Asia. *Journal of Climate*, *10*(6), 1393–1404. https://doi.org/10.1175/1520-0442(1997)010<1393:CAHCIT>2.0.CO;2

Alonso-Zarza, A. M. (2003). Palaeoenvironmental significance of palustrine carbonates and calcretes in the geological record. *Earth-Science Reviews*, *60*(3–4), 261–298. https://doi.org/10.1016/S0012-8252(02)00106-X

Alonso-Zarza, A. M., & Wright, V. P. (2010). Palustrine carbonates. *Developments in Sedimentology*, *61*, 103–131. https://doi.org/10.1016/S0070-4571(09)06102-0

Alonso-Zarza, A. M., Wright, V. P., Calvo, J. P., & Del Cura, M. G. (1992). Soil-landscape and climatic relationships in the middle Miocene of the Madrid Basin. *Sedimentology*, *39*(1), 17–35. https://doi.org/10.1111/j.1365-3091.1992.tb01021.x

Bakirov, A. B., & Maksumova, R. A. (2001). Geology and evolution of the Tien Shan lithosphere (in Russian). *Russian Geology and Geophysics*, *42*, 1359–1366.

Balco, G., & Rovey, C. W. (2008). An isochron method for cosmogenic-nuclide dating of buried soils and sediments. *American Journal of Science*, *308*(10), 1083–1114. https://doi.org/10.2475/10.2008.02

Balco, G., Stone, J. O., Lifton, N. A., & Dunai, T. J. (2008). A complete and easily accessible means of calculating surface exposure ages or erosion rates from 10Be and 26Al measurements. *Quaternary Geochronology*, *3*, 174–195. https://doi.org/10.1016/j.quageo.2007.12.001

Baldwin, J., & Vecchi, G. (2016). Influence of the Tian Shan on arid extratropical Asia. *Journal of Climate*, *29*(16), 5741–5762. https://doi.org/10.1175/JCLI-D-15-0490.1

Bazhenov, M. L., Burtman, V. S., & Dvorova, A. V. (1999). Permian paleomagnetism of the Tien Shan fold belt, Central Asia: Post-collisional rotations and deformation. *Tectonophysics*, *312*(2–4), 303–329. https://doi.org/10.1016/S0040-1951(99)00181-X

Bazhenov, M. L., & Mikolaichuk, A. V. (2004). Structural evolution of Central Asia to the north of Tibet: A synthesis of paleomagnetic and geological data. *Geotectonics*, *38*(5), 379–393.

Bershaw, J., & Lechler, A. R. (2019). The isotopic composition of meteoric water along altitudinal transects in the Tian Shan of Central Asia. *Chemical Geology*, *516*, 68–78. https://doi.org/10.1016/j.chemgeo.2019.03.032

Biske, Y. S. (1996). *Paleozoic structure and history of southern Tien Shan* (p. 187). Saint Petersburg State University (in Russian).

Biske, Y. S., & Seltmann, R. (2010). Paleozoic Tian-Shan as a transitional region between the Rheic and Urals-Turkestan oceans. *Gondwana Research*, *17*(2–3), 602–613. https://doi.org/10.1016/j.gr.2009.11.014

Bookhagen, B., & Burbank, D. W. (2010). Toward a complete Himalayan hydrological budget: Spatiotemporal distribution of snowmelt and rainfall and their impact on river discharge. *Journal of Geophysical Research: Earth Surface*, *115*(F3), 1–25. https://doi.org/10.1029/2009JF001426

Bookhagen, B., & Strecker, M. R. (2008). Orographic barriers, high-resolution TRMM rainfall, and relief variations along the eastern Andes. *Geophysical Research Letters*, *35*(6), 1–6. https://doi.org/10.1029/2007GL032011

Bosboom, R., Mandic, O., Dupont-Nivet, G., Proust, J. N., Ormukov, C., & Aminov, J. (2017). Late Eocene palaeogeography of the proto-Paratethys Sea in Central Asia (NW China, southern Kyrgyzstan and SW Tajikistan). *Geological Society, London, Special Publications*, *427*(1), 565–588. https://doi.org/10.1144/SP427.11

Bosboom, R. E., Abels, H. A., Hoorn, C., van den Berg, B. C., Guo, Z., & Dupont-Nivet, G. (2014). Aridification in continental Asia after the middle Eocene climatic optimum (MECO). *Earth and Planetary Science Letters*, *389*, 34–42. https://doi.org/10.1016/j.epsl.2013.12.014

Bosboom, R. E., Dupont-Nivet, G., Grothe, A., Brinkhuis, H., Villa, G., Mandic, O., Stoica, M., Huang, W., Yang, W., Guo, Z., & Krijgsman, W. (2014). Linking Tarim Basin sea retreat (West China) and Asian aridification in the late Eocene. *Basin Research*, *26*(5), 621–640. https://doi.org/10.1111/bre.12054

Bougeois, L., Dupont-Nivet, G., de Rafélis, M., Tindall, J. C., Proust, J. N., Reichart, G. J., de Nooijer, L. J., Guo, Z., & Ormukov, C. (2018). Asian monsoons and aridification response to Paleogene Sea retreat and Neogene westerly shielding indicated by seasonality in Paratethys oysters. *Earth and Planetary Science Letters*, *485*, 99–110. https://doi.org/10.1016/j.epsl.2017.12.036

Bowman, D., Korjenkov, A., Porat, N., & Czassny, B. (2004). Morphological response to quaternary deformation at an intermontane basin piedmont, the northern Tien Shan, Kyrghyzstan. *Geomorphology*, *63*(1–2), 1–24. https://doi.org/10.1016/j.geomorph.2004.03.007

Breecker, D. O., Sharp, Z. D., & McFadden, L. D. (2009). Seasonal bias in the formation and stable isotopic composition of pedogenic carbonate in modern soils from Central New Mexico, USA. *Geological Society of America Bulletin*, *121*(3–4), 630–640. https://doi.org/10.1130/B26413.1

Bullen, M. E., Burbank, D. W., & Garver, J. I. (2003). Building the northern Tien Shan: Integrated thermal, structural, and topographic constraints. *The Journal of Geology*, *111*(2), 149–165. https://doi.org/10.1086/345840

Bullen, M. E., Burbank, D. W., Garver, J. I., & Abdrakhmatov, K. Y. (2001). Late Cenozoic tectonic evolution of the northwestern Tien Shan: New age estimates for the initiation of mountain building. *Geological Society of America Bulletin*, *113*(12), 1544–1559. https://doi.org/10.1130/0016-7606(2001)113<1544:LCTEOT>2.0.CO;2

Burgette, R. J., Weldon, R. J., II, Abdrakhmatov, K. Y., Ormukov, C., Owen, L. A., & Thompson, S. C. (2017). Timing and process of river and lake terrace formation in the Kyrgyz Tien Shan. *Quaternary Science Reviews*, *159*, 15–34. https://doi.org/10.1016/j.quascirev.2017.01.003

Caves, J. K., Bayshashov, B. U., Zhamangara, A., Ritch, A. J., Ibarra, D. E., Sjostrom, D. J., Mix, H. T., Winnick, M. J., & Chamberlain, C. P. (2017). Late Miocene uplift of the Tian Shan and Altai and reorganization of Central Asia climate. *GSA Today*, *27*(2), 19–26. https://doi.org/10.1130/GSATG305A.1

Caves, J. K., Moragne, D. Y., Ibarra, D. E., Bayshashov, B. U., Gao, Y., Jones, M. M., Zhamangara, A., Arzhannikova, A. V., Arzhannikov, S. G., & Chamberlain, C. P. (2016). The Neogene de-greening of Central Asia. *Geology*, *44*(11), 887–890. https://doi.org/10.1130/G38267.1

Caves, J. K., Sjostrom, D. J., Mix, H. T., Winnick, M. J., & Chamberlain, C. P. (2014). Aridification of Central Asia and uplift of the Altai and Hangay Mountains, Mongolia: Stable isotope evidence. *American Journal of Science*, *314*(8), 1171–1201. https://doi.org/10.2475/08.2014.01

Caves, J. K., Winnick, M. J., Graham, S. A., Sjostrom, D. J., Mulch, A., & Chamberlain, C. P. (2015). Role of the westerlies in Central Asia climate over the Cenozoic. *Earth and Planetary Science Letters*, *428*, 33–43. https://doi.org/10.1016/j.epsl.2015.07.023

Caves Rugenstein, J. K., & Chamberlain, C. P. (2018). The evolution of hydroclimate in Asia over the Cenozoic: A stable-isotope perspective. *Earth-Science Reviews*, *185*, 1129–1156. https://doi.org/10.1016/j.earscirev.2018.09.003

Cerling, T. E. (1984). The stable isotopic composition of modern soil carbonate and its relationship to climate. *Earth and Planetary Science Letters*, *71*(2), 229–240. https://doi.org/10.1016/0012-821X(84)90089-X

Cerling, T. E., Harris, J. M., MacFadden, B. J., Leakey, M. G., Quade, J., Eisenmann, V., & Ehleringer, J. R. (1997). Global vegetation change through the Miocene/Pliocene boundary. *Nature*, *389*(6647), 153–158. https://doi.org/10.1038/38229

Cerling, T. E., & Quade, J. (1993). Stable carbon and oxygen isotopes in soil carbonates. *Climate change in continental isotopic records. Geophysical Monograph*, *78*, 217–231. https://doi.org/10.1029/GM078p0217

Chamberlain, C. P., Mix, H. T., Mulch, A., Hren, M. T., Kent-Corson, M. L., Davis, S. J., Horton, T. W., & Graham, S. A. (2012). The Cenozoic climatic and topographic evolution of the western north American cordillera. *American Journal of Science*, *312*(2), 213–262. https://doi.org/10.2475/02.2012.05

Chamberlain, C. P., & Poage, M. A. (2000). Reconstructing the paleotopography of mountain belts from the isotopic composition of authigenic minerals. *Geology*, *28*(2), 115–118. https://doi.org/10.1130/0091-7613(2000)28<115:RTPOMB>2.0.CO;2

Chang, J., Glorie, S., Qiu, N., Min, K., Xiao, Y., & Xu, W. (2021). Late Miocene (10.0~6.0 Ma) rapid exhumation of the Chinese south Tianshan: Implications for the timing of aridification in the Tarim Basin. *Geophysical Research Letters*, *48*(3), e2020GL090623. https://doi.org/10.1029/2020GL090623

Charreau, J., Blard, P. H., Puchol, N., Avouac, J. P., Lallier-Vergès, E., Bourlès, D., Braucher, R., Gallaud, A., Finkel, R., Jolivet, M., & Chen, Y. (2011). Paleo-erosion rates in Central Asia since 9 Ma: A transient increase at the onset of quaternary glaciations? *Earth and Planetary Science Letters*, *304*(1–2), 85–92. https://doi.org/10.1016/j.epsl.2011.01.018

Charreau, J., Gumiaux, C., Avouac, J. P., Augier, R., Chen, Y., Barrier, L., Gilder, S., Dominguez, S., Charles, N., & Wang, Q. (2009). The Neogene Xiyu formation, a diachronous prograding gravel wedge at front of the Tianshan: Climatic and tectonic implications. *Earth and Planetary Science Letters*, *287*(3–4), 298–310. https://doi.org/10.1016/j.epsl.2009.07.035

Charreau, J., Kent-Corson, M. L., Barrier, L., Augier, R., Ritts, B. D., Chen, Y., France-Lannord, C., & Guilmette, C. (2012). A high-resolution stable isotopic record from the Junggar Basin (NW China): Implications for the paleotopographic evolution of the Tianshan Mountains. *Earth and Planetary Science Letters*, *341*, 158–169. https://doi.org/10.1016/j.epsl.2012.05.033

Chen, J., Burbank, D. W., Scharer, K. M., Sobel, E., Yin, J., Rubin, C., & Zhao, R. (2002). Magnetochronology of the upper Cenozoic strata in the southwestern Chinese Tian Shan: Rates of Pleistocene folding and thrusting. *Earth and Planetary Science Letters*, *195*(1–2), 113–130. https://doi.org/10.1016/S0012-821X(01)00579-9

Child, D., Elliott, G., Mifsud, C., Smith, A. M., & Fink, D. (2000). Sample processing for earth science studies at ANTARES. *Nuclear Instruments and Methods in Physics Research Section B: Beam Interactions with Materials and Atoms*, *172*(1–4), 856–860. https://doi.org/10.1016/S0168-583X(00)00198-1

Chmeleff, J., von Blanckenburg, F., Kossert, K., & Jakob, D. (2010). Determination of the ^{10}Be half-life by multicollector ICP-MS and liquid scintillation counting. *Nuclear Instruments and Methods in Physics Research Section B: Beam Interactions with Materials and Atoms*, *268*(2), 192–199. https://doi.org/10.1016/j.nimb.2009.09.012

Codilean, A. T., & Sadler, P. M. (2021). Tectonic controls on Himalayan denudation? *AGU Advances*, *2*(3), e2021AV000539. https://doi.org/10.1029/2021AV000539

Corbett, L. B., Bierman, P. R., Rood, D. H., Caffee, M. W., Lifton, N. A., & Woodruff, T. E. (2017). Cosmogenic ^{26}Al/^{10}Be surface production ratio in Greenland. *Geophysical Research Letters*, *44*(3), 1350–1359. https://doi.org/10.1002/2016GL071276

De Batist, M., Imbo, Y., Vermeesch, P., Klerkx, J., Giralt, S., Delvaux, D., Lignier, V., Beck, C., Kalugin, I., & Abdrakhmatov, K. E. (2002). Bathymetry and sedimentary environments of Lake Issyk-Kul, Kyrgyz Republic (Central Asia): A large, high-altitude, tectonic lake. In *Lake Issyk-Kul: Its natural environment* (pp. 101–123). Springer. https://doi.org/10.1007/978-94-010-0491-6_9

De Grave, J., Glorie, S., Buslov, M. M., Stockli, D. F., McWilliams, M. O., & Batalev, V. Y. (2013). Thermo-tectonic history of the Issyk-Kul basement (Kyrgyz northern Tien Shan, Central Asia). *Gondwana Research*, *23*(3), 998–1020. https://doi.org/10.1016/j.gr.2012.06.014

De Pelsmaeker, E., Glorie, S., Buslov, M. M., Zhimulev, F. I., Poujol, M., Korobkin, V. V., Vanhaecke, F., Vetrov, E. V., & De Grave, J. (2015). Late-Paleozoic emplacement and Meso-Cenozoic reactivation of the southern Kazakhstan granitoid basement. *Tectonophysics*, *662*, 416–433. https://doi.org/10.1016/j.tecto.2015.06.014

Dettman, D. L., Fang, X., Garzione, C. N., & Li, J. (2003). Uplift-driven climate change at 12 Ma: A long δ^{18}O record from the NE margin of the Tibetan plateau. *Earth and Planetary Science Letters*, *214*(1–2), 267–277. https://doi.org/10.1016/S0012-821X(03)00383-2

Dupont-Nivet, G., Krijgsman, W., Langereis, C. G., Abels, H. A., Dai, S., & Fang, X. (2007). Tibetan plateau aridification linked to global cooling at the Eocene–Oligocene transition. *Nature*, *445*(7128), 635–638. https://doi.org/10.1038/nature05516

Erlanger, E. D., Granger, D. E., & Gibbon, R. J. (2012). Rock uplift rates in South Africa from isochron burial dating of fluvial and marine terraces. *Geology*, *40*(11), 1019–1022. https://doi.org/10.1130/G33172.1

Fan, M., Dettman, D. L., Song, C., Fang, X., & Garzione, C. N. (2007). Climatic variation in the Linxia basin, NE Tibetan plateau, from 13.1 to 4.3 Ma: The stable isotope record. *Palaeogeography, Palaeoclimatology, Palaeoecology*, *247*(3–4), 313–328. https://doi.org/10.1016/j.palaeo.2006.11.001

Fang, X., An, Z., Clemens, S. C., Zan, J., Shi, Z., Yang, S., & Han, W. (2020). The 3.6-Ma aridity and westerlies history over midlatitude Asia linked with global climatic cooling. *Proceedings of the National Academy of Sciences of the United States of America*, *117*(40), 24729–24734. https://doi.org/10.1073/pnas.1922710117

Fortuna, A. B. (2016). Paleogene and Neogene paleoclimate in the northern Tian Shan (in Russian). *Vestnik IS NAN KR*, *1*(7), 102–111.

Fortuna, A. B., Abdieva, S. V., & Korzhenkov, A. M. (2017). The history of flora and vegetation development in the Issyk Kul basin during the Cenozoic (in Russian). *Vestnik KRSU*, *17*(8), 201–205.

Fortuna, A. B., Kerimbekov, C. K., Kuzikov, S. I., & Mikolaichuk, A. V. (1994). Lithostratigraphic and palynologic data of Cenozoic deposits of Tessik-Sarybulak depression (in Russian). In O. K. Chediya (Ed.), *Geology of Cenozoic and seismotectonics of the Tien Shan* (pp. 26–39). Frunse, Ilim.

Freytet, P., & Verrecchia, E. P. (2002). Lacustrine and palustrine carbonate petrography: An overview. *Journal of Paleolimnology*, *27*(2), 221–237. https://doi.org/10.1023/A:1014263722766

Frisch, K., Voigt, S., Verestek, V., Appel, E., Albert, R., Gerdes, A., Arndt, I., Raddatz, J., Voigt, T., Weber, Y., & Batenburg, S. J. (2019). Long-period astronomical forcing of westerlies' strength in Central Asia during Miocene climate cooling. *Paleoceanography and Paleoclimatology*, *34*(11), 1784–1806. https://doi.org/10.1029/2019PA003642

Frisch, K., Voigt, S., Voigt, T., Hellwig, A., Verestek, V., & Weber, Y. (2019). Extreme aridity prior to lake expansion deciphered from facies evolution in the Miocene Ili Basin, south-East Kazakhstan. *Sedimentology*, *66*(5), 1716–1745.

Fujioka, T., Fink, D., & Mifsud, C. (2015). Towards improvement of aluminium assay in quartz for in situ cosmogenic ^{26}Al analysis at ANSTO. *Nuclear Instruments and Methods in Physics Research Section B: Beam Interactions with Materials and Atoms*, *361*, 346–353. https://doi.org/10.1016/j.nimb.2015.07.120

Garzione, C. N., Dettman, D. L., & Horton, B. K. (2004). Carbonate oxygen isotope paleoaltimetry: Evaluating the effect of diagenesis on paleoelevation estimates for the Tibetan plateau. *Palaeogeography, Palaeoclimatology, Palaeoecology*, *212*(1–2), 119–140. https://doi.org/10.1016/j.palaeo.2004.05.020

Gebhardt, A. C., Naudts, L., De Mol, L., Klerkx, J., Abdrakhmatov, K., Sobel, E. R., & De Batist, M. (2017). High-amplitude lake-level changes in tectonically active Lake Issyk-Kul (Kyrgyzstan) revealed by high-resolution seismic reflection data. *Climate of the Past*, *13*(1), 73–92. https://doi.org/10.5194/cp-13-73-2017

Glorie, S., & De Grave, J. (2016). Exhuming the Meso–Cenozoic Kyrgyz Tianshan and Siberian Altai-Sayan: A review based on low-temperature thermochronology. *Geoscience Frontiers*, *7*(2), 155–170. https://doi.org/10.1016/j.gsf.2015.04.003

Graham, S. A., Chamberlain, C. P., Yue, Y., Ritts, B. D., Hanson, A. D., Horton, T. W., Waldbauer, J. R., Poage, M. A., & Feng, X. (2005). Stable isotope records of Cenozoic climate and topography, Tibetan plateau and Tarim basin. *American Journal of Science*, *305*(2), 101–118. https://doi.org/10.2475/ajs.305.2.101

Granger, D. E., & Muzikar, P. F. (2001). Dating sediment burial with in situ-produced cosmogenic nuclides: Theory, techniques, and limitations. *Earth and Planetary Science Letters*, *188*(1–2), 269–281. https://doi.org/10.1016/S0012-821X(01)00309-0

Grigina, O. M., & Fortuna, A. B. (1975). Main stages of the vegetation development in the Issyk Kul basin in the Cenozoic (in Russian). In *History of lakes and inland seas in arid zone: Thesis* (Vol. *4*, pp. 79–85). Leningrad.

Grigina, O. M., & Fortuna, A. B. (1981). *Paleogeography of the northern Tian Shan in the Cenozoic* (in Russian). Frunse.

Halsted, C. T., Bierman, P. R., & Balco, G. (2021). Empirical evidence for latitude and altitude variation of the In situ Cosmogenic ^{26}Al/^{10}Be production ratio. *Geosciences*, *11*(10), 402. https://doi.org/10.3390/geosciences11100402

Heermance, R. V., Chen, J., Burbank, D. W., & Wang, C. (2007). Chronology and tectonic controls of late tertiary deposition in the southwestern Tian Shan foreland, NW China. *Basin Research*, *19*(4), 599–632. https://doi.org/10.1111/j.1365-2117.2007.00339.x

Hellwig, A., Voigt, S., Mulch, A., Frisch, K., Bartenstein, A., Pross, J., Gerdes, A., & Voigt, T. (2018). Late Oligocene to early Miocene humidity change recorded in terrestrial sequences in the Ili Basin (South-Eastern Kazakhstan, Central Asia). *Sedimentology*, *65*(2), 517–539. https://doi.org/10.1111/sed.12390

Herbert, T. D., Lawrence, K. T., Tzanova, A., Peterson, L. C., Caballero-Gill, R., & Kelly, C. S. (2016). Late Miocene global

cooling and the rise of modern ecosystems. *Nature Geoscience*, *9*(11), 843–847. https://doi.org/10.1038/ngeo2813

Hough, B. G., Garzione, C. N., Wang, Z., Lease, R. O., Burbank, D. W., & Yuan, D. (2011). Stable isotope evidence for topographic growth and basin segmentation: Implications for the evolution of the NE Tibetan plateau. *Bulletin*, *123*(1–2), 168–185. https://doi.org/10.1130/B30090.1

Jia, Y., Wu, H., Zhu, S., Li, Q., Zhang, C., Yu, Y., & Sun, A. (2020). Cenozoic aridification in Northwest China evidenced by paleovegetation evolution. *Palaeogeography, Palaeoclimatology, Palaeoecology*, *557*, 109907. https://doi.org/10.1016/j.palaeo.2020.109907

Kaya, M. Y., Dupont-Nivet, G., Proust, J. N., Roperch, P., Bougeois, L., Meijer, N., Frieling, J., Fioroni, C., Altiner, S. Ö., Vardar, E., & Barbolini, N. (2019). Paleogene evolution and demise of the proto-Parathys Sea in Central Asia (Tarim and Tajik basins): Role of intensified tectonic activity at ca. 41 Ma. *Basin Research*, *31*(3), 461–486. https://doi.org/10.1111/bre.12330

Kent-Corson, M. L., Ritts, B. D., Zhuang, G., Bovet, P. M., Graham, S. A., & Chamberlain, C. P. (2009). Stable isotopic constraints on the tectonic, topographic, and climatic evolution of the northern margin of the Tibetan plateau. *Earth and Planetary Science Letters*, *282*(1–4), 158–166. https://doi.org/10.1016/j.epsl.2009.03.011

Knudsen, M. F., Nørgaard, J., Grischott, R., Kober, F., Egholm, D. L., Hansen, T. M., & Jansen, J. D. (2020). New cosmogenic nuclide burial-dating model indicates onset of major glaciations in the Alps during middle Pleistocene transition. *Earth and Planetary Science Letters*, *549*, 116491. https://doi.org/10.1016/j.epsl.2020.116491

Kohl, C. P., & Nishiizumi, K. (1992). Chemical isolation of quartz for measurement of in-situ-produced cosmogenic nuclides. *Geochimica et Cosmochimica Acta*, *56*(9), 3583–3587. https://doi.org/10.1016/0016-7037(92)90401-4

Korschinek, G., Bergmaier, A., Faestermann, T., Gerstmann, U. C., Knie, K., Rugel, G., Wallner, A., Dillmann, I., Dollinger, G., Von Gosstomski, C. L., Kossert, K., Maiti, M., Poutivtsev, M., & Remmert, A. (2010). A new value for the half-life of ^{10}Be by heavy-ion elastic recoil detection and liquid scintillation counting. *Nuclear Instruments and Methods in Physics Research Section B: Beam Interactions with Materials and Atoms*, *268*(2), 187–191. https://doi.org/10.1016/j.nimb.2009.09.020

Lal, D. (1991). Cosmic ray labeling of erosion surfaces: In situ nuclide production rates and erosion models. *Earth and Planetary Science Letters*, *104*(2–4), 424–439. https://doi.org/10.1016/0012-821X(91)90220-C

Lauterbach, S., Witt, R., Plessen, B., Dulski, P., Prasad, S., Mingram, J., Gleixner, G., Hettler-Riedel, S., Stebich, M., Schnetger, B., Schwalb, A., & Schwarz, A. (2014). Climatic imprint of the mid-latitude westerlies in the Central Tian Shan of Kyrgyzstan and teleconnections to North Atlantic climate variability during the last 6000 years. *The Holocene*, *24*(8), 970–984. https://doi.org/10.1177/0959683614534741

Leng, M. J., & Marshall, J. D. (2004). Palaeoclimate interpretation of stable isotope data from lake sediment archives. *Quaternary Science Reviews*, *23*(7–8), 811–831. https://doi.org/10.1016/j.quascirev.2003.06.012

Levin, N. E., Cerling, T. E., Passey, B. H., Harris, J. M., & Ehleringer, J. R. (2006). A stable isotope aridity index for terrestrial environments. *Proceedings of the National Academy of Sciences of*

the United States of America, *103*(30), 11201–11205. https://doi.org/10.1073/pnas.0604719103

Li, B., Sun, D., Wang, X., Zhang, Y., Hu, W., Wang, F., Li, Z., Ma, Z., & Liang, B. (2016). $\delta^{18}O$ and $\delta^{13}C$ records from a Cenozoic sedimentary sequence in the Lanzhou Basin, northwestern China: Implications for palaeoenvironmental and palaeoecological changes. *Journal of Asian Earth Sciences*, *125*, 22–36. https://doi.org/10.1016/j.jseaes.2016.05.010

Li, H. C., & Ku, T. L. (1997). $\delta^{13}C$–$\delta^{18}O$ covariance as a paleohydrological indicator for closed-basin lakes. *Palaeogeography, Palaeoclimatology, Palaeoecology*, *133*(1–2), 69–80. https://doi.org/10.1016/S0031-0182(96)00153-8

Li, J. X., Yue, L. P., Roberts, A. P., Hirt, A. M., Pan, F., Guo, L., Xu, Y., Xi, R. G., Guo, L., Qiang, X. K., Gai, C. C., Jiang, Z. X., Sun, Z. M., & Liu, Q. S. (2018). Global cooling and enhanced Eocene Asian mid-latitude interior aridity. *Nature Communications*, *9*(1), 1–8. https://doi.org/10.1038/s41467-018-05415-x

Licht, A., Dupont-Nivet, G., Pullen, A., Kapp, P., Abels, H. A., Lai, Z., Guo, Z., Abell, J., & Giesler, D. (2016). Resilience of the Asian atmospheric circulation shown by Paleogene dust provenance. *Nature Communications*, *7*(1), 1–6. https://doi.org/10.1038/ncomms12390

Liu, W., Liu, Z., An, Z., Sun, J., Chang, H., Wang, N., Dong, J., & Wang, H. (2014). Late Miocene episodic lakes in the arid Tarim Basin, western China. *Proceedings of the National Academy of Sciences of the United State of America*, *111*(46), 16292–16296. https://doi.org/10.1073/pnas.1410890111

Macaulay, E. A., Sobel, E. R., Mikolaichuk, A., Kohn, B., & Stuart, F. M. (2014). Cenozoic deformation and exhumation history of the central Kyrgyz Tien Shan. *Tectonics*, *33*(2), 135–165. https://doi.org/10.1002/2013TC003376

Macaulay, E. A., Sobel, E. R., Mikolaichuk, A., Landgraf, A., Kohn, B., & Stuart, F. (2013). Thermochronologic insight into late Cenozoic deformation in the basement-cored Terskey range, Kyrgyz Tien Shan. *Tectonics*, *32*(3), 487–500. https://doi.org/10.1002/tect.20040

Macaulay, E. A., Sobel, E. R., Mikolaichuk, A. V., Wack, M., Gilder, S. A., Mulch, A., Fortuna, A. B., Hynek, S., & Apayarov, F. (2016). The sedimentary record of the Issyk Kul basin, Kyrgyzstan: Climatic and tectonic inferences. *Basin Research*, *28*(1), 57–80. https://doi.org/10.1111/bre.12098

Maksumova, R. A., Djenchuraeva, A. V., & Berezanskii, A. V. (2001). Structure and evolution of the Tien Shan nappe-folded orogen. *Russian Geology and Geophysics*, *42*, 1367–1374.

Methner, K., Fiebig, J., Wacker, U., Umhoefer, P., Chamberlain, C. P., & Mulch, A. (2016). Eocene-Oligocene proto-cascades topography revealed by clumped ($\Delta47$) and oxygen isotope ($\delta^{18}O$) geochemistry (Chumstick Basin, WA, USA). *Tectonics*, *35*(3), 546–564. https://doi.org/10.1002/2015TC003984

Miao, Y., Herrmann, M., Wu, F., Yan, X., & Yang, S. (2012). What controlled Mid–Late Miocene long-term aridification in Central Asia? Global cooling or Tibetan Plateau uplift: A review. *Earth-Science Reviews*, *112*(3–4), 155–172. https://doi.org/10.1016/j.earscirev.2012.02.003

Molnar, P., & Tapponnier, P. (1975). Cenozoic tectonics of Asia: Effects of a continental collision: Features of recent continental tectonics in Asia can be interpreted as results of the India-Eurasia collision. *Science*, *189*(4201), 419–426. https://doi.org/10.1126/science.189.4201.419

Mulch, A. (2016). Stable isotope paleoaltimetry and the evolution of landscapes and life. *Earth and Planetary Science Letters*, *433*, 180–191. https://doi.org/10.1016/j.epsl.2015.10.034

Nishiizumi, K. (2004). Preparation of ^{26}Al AMS standards. *Nuclear Instruments and Methods in Physics Research Section B: Beam Interactions with Materials and Atoms*, *223*, 388–392. https://doi.org/10.1016/j.nimb.2004.04.075

Nishiizumi, K., Imamura, M., Caffee, M. W., Southon, J. R., Finkel, R. C., & McAninch, J. (2007). Absolute calibration of ^{10}Be AMS standards. *Nuclear Instruments and Methods in Physics Research Section B: Beam Interactions with Materials and Atoms*, *258*(2), 403–413. https://doi.org/10.1016/j.nimb.2007.01.297

Norris, T. L., Gancarz, A. J., Rokop, D. J., & Thomas, K. W. (1983). Half-life of ^{26}Al. *Journal of Geophysical Research: Solid Earth*, *88*(S01), B331–B333. https://doi.org/10.1029/JB088iS01p0B331

Oberhänsli, H., & Molnar, P. (2012). Climate evolution in Central Asia during the past few million years: A case study from Issyk Kul. *Scientific Drilling*, *13*, 51–57. https://doi.org/10.2204/iodp.sd.13.09.2011

Omuraliev, M., & Omuralieva, A. (2004). *Late Cenozoic tectonics of the Tien Shan*. Institute of Seizmology, National Academy of Sciences Kyrgyz Republic, Bishkek.

Poage, M. A., & Chamberlain, C. P. (2001). Empirical relationships between elevation and the stable isotope composition of precipitation and surface waters: Considerations for studies of paleoelevation change. *American Journal of Science*, *301*(1), 1–15. https://doi.org/10.2475/ajs.301.1.1

Prud'homme, C., Scardia, G., Vonhof, H., Guinoiseau, D., Nigmatova, S., Fiebig, J., Gerdes, A., Janssen, R., & Fitzsimmons, K. E. (2021). Central Asian modulation of northern hemisphere moisture transfer over the late Cenozoic. *Communications Earth & Environment*, *2*(1), 1–8. https://doi.org/10.1038/s43247-021-00173-z

Quade, J., Breecker, D. O., Daëron, M., & Eiler, J. (2011). The paleoaltimetry of Tibet: An isotopic perspective. *American Journal of Science*, *311*(2), 77–115. https://doi.org/10.2475/02.2011.01

Quade, J., Leary, R., Dettinger, M. P., Orme, D., Krupa, A., DeCelles, P. G., Kano, A., Kato, H., Waldrip, R., Huang, W., & Kapp, P. (2020). Resetting southern Tibet: The serious challenge of obtaining primary records of Paleoaltimetry. *Global and Planetary Change*, *191*, 103194. https://doi.org/10.1016/j.gloplacha.2020.103194

Ramstein, G., Fluteau, F., Besse, J., & Joussaume, S. (1997). Effect of orogeny, plate motion and land–sea distribution on Eurasian climate change over the past 30 million years. *Nature*, *386*(6627), 788–795. https://doi.org/10.1038/386788a0

Ricketts, R. D., Johnson, T. C., Brown, E. T., Rasmussen, K. A., & Romanovsky, V. V. (2001). The Holocene paleolimnology of Lake Issyk-Kul, Kyrgyzstan: Trace element and stable isotope composition of ostracodes. *Palaeogeography, Palaeoclimatology, Palaeoecology*, *176*(1–4), 207–227. https://doi.org/10.1016/S0031-0182(01)00339-X

Rosenwinkel, S., Landgraf, A., Schwanghart, W., Volkmer, F., Dzhumabaeva, A., Merchel, S., Rugel, G., Preusser, F., & Korup, O. (2017). Late Pleistocene outburst floods from Issyk Kul, Kyrgyzstan? *Earth Surface Processes and Landforms*, *42*(10), 1535–1548. https://doi.org/10.1002/esp.4109

Roud, S. C., Wack, M. R., Gilder, S. A., Kudriavtseva, A., & Sobel, E. R. (2021). Miocene to early Pleistocene depositional history

and tectonic evolution of the Issyk-Kul Basin, Central Tian Shan. *Geochemistry, Geophysics, Geosystems*, *22*(4), e2020GC009556. https://doi.org/10.1029/2020GC009556

Rowley, D. B., & Garzione, C. N. (2007). Stable isotope-based paleoaltimetry. *Annual Review of Earth and Planetary Sciences*, *35*, 463–508. https://doi.org/10.1146/annurev.earth.35.031306.140155

Sanyal, P., Bhattacharya, S. K., & Prasad, M. (2005). Chemical diagenesis of Siwalik sandstone: Isotopic and mineralogical proxies from Surai Khola section, Nepal. *Sedimentary Geology*, *180*(1–2), 57–74. https://doi.org/10.1016/j.sedgeo.2005.06.005

Schaefer, J. M., Codilean, A. T., Willenbring, J. K., Lu, Z.-T., Keisling, B., Fülöp, R.-H., & Val, P. (2022). Cosmogenic nuclide techniques. *Nature Reviews Methods Primers*, *2*, 18. https://doi.org/10.1038/s43586-022-00096-9

Schwarz, A., Turner, F., Lauterbach, S., Plessen, B., Krahn, K. J., Glodniok, S., Mischke, S., Stebich, M., Witt, R., Mingram, J., & Schwalb, A. (2017). Mid-to late Holocene climate-driven regime shifts inferred from diatom, ostracod and stable isotope records from Lake son Kol (Central Tian Shan, Kyrgyzstan). *Quaternary Science Reviews*, *177*, 340–356. https://doi.org/10.1016/j.quascirev.2017.10.009

Selander, J., Oskin, M., Ormukov, C., & Abdrakhmatov, K. (2012). Inherited strike-slip faults as an origin for basement-cored uplifts: Example of the Kungey and Zailiskey ranges, northern Tian Shan. *Tectonics*, *31*(4), 1–22. https://doi.org/10.1029/2011TC003002

Seltmann, R., Konopelko, D., Biske, G., Divaev, F., & Sergeev, S. (2011). Hercynian post-collisional magmatism in the context of Paleozoic magmatic evolution of the Tien Shan orogenic belt. *Journal of Asian Earth Sciences*, *42*, 821–838. https://doi.org/10.1016/j.jseaes.2010.08.016

Sobel, E. R., Chen, J., & Heermance, R. V. (2006). Late Oligocene–Early Miocene initiation of shortening in the Southwestern Chinese Tian Shan: Implications for Neogene shortening rate variations. *Earth and Planetary Science Letters*, *247*(1–2), 70–81. https://doi.org/10.1016/j.epsl.2006.03.048

Sobel, E. R., Oskin, M., Burbank, D., & Mikolaichuk, A. (2006). Exhumation of basement-cored uplifts: Example of the Kyrgyz range quantified with apatite fission track thermochronology. *Tectonics*, *25*(2), 1–17. https://doi.org/10.1029/2005TC001809

Spötl, C., & Vennemann, T. W. (2003). Continuous-flow isotope ratio mass spectrometric analysis of carbonate minerals. *Rapid Communications in Mass Spectrometry*, *17*(9), 1004–1006. https://doi.org/10.1002/rcm.1010

Sun, J., Gong, Z., Tian, Z., Jia, Y., & Windley, B. (2015). Late Miocene stepwise aridification in the Asian interior and the interplay between tectonics and climate. *Palaeogeography, Palaeoclimatology, Palaeoecology*, *421*, 48–59. https://doi.org/10.1016/j.palaeo.2015.01.001

Swart, P. K. (2015). The geochemistry of carbonate diagenesis: The past, present and future. *Sedimentology*, *62*(5), 1233–1304. https://doi.org/10.1111/sed.12205

Talbot, M. R. (1990). A review of the palaeohydrological interpretation of carbon and oxygen isotopic ratios in primary lacustrine carbonates. *Chemical Geology: Isotope Geoscience Section*, *80*(4), 261–279. https://doi.org/10.1016/0168-9622(90)90009-2

Tursungasiev, B. T., & Petrov, O. V. (Eds.). (2008). *Geological map of Kyrgyzstan of 1:500000 scales*. Russian Geological Research Institute (VSEGEI).

Voigt, S., Weber, Y., Frisch, K., Bartenstein, A., Hellwig, A., Petschick, R., Bahr, A., Pross, J., Koutsodendris, A., Voigt, T., Verestek, V., & Appel, E. (2017). Climatically forced moisture supply, sediment flux and pedogenesis in Miocene mudflat deposits of south-East Kazakhstan, Central Asia. *The Depositional Record*, *3*(2), 209–232. https://doi.org/10.1002/dep2.34

von Blanckenburg, F., Belshaw, N. S., & O'Nions, R. K. (1996). Separation of ^{9}Be and cosmogenic ^{10}Be from environmental materials and SIMS isotope dilution analysis. *Chemical Geology*, *129*(1–2), 93–99. https://doi.org/10.1016/0009-2541(95)00157-3

Voskresenskaya, T. N. (2013). Lacustrine sediments and paleogeography in the Issyk Kul basin in the Cenozoic (in Russian). In *Sedimentary basins, sedimentary and postsedimentary processes in the geological history* (Vol. *1*, pp. 180–183). INGG SO RAN.

Voskresenskaya, T. N., & Leflat, O. N. (2015). Paleogeographic evolution of the Issyk Kul basin during the Pleistocene (in Russian). *Vestnik Moskovskogo Universiteta. Seriya 5, Geografiya*, 71–77.

Wack, M. R., Gilder, S. A., Macaulay, E. A., Sobel, E. R., Charreau, J., & Mikolaichuk, A. (2014). Cenozoic magnetostratigraphy and magnetic properties of the southern Issyk-Kul basin, Kyrgyzstan. *Tectonophysics*, *629*, 14–26. https://doi.org/10.1016/j.tecto.2014.03.030

Wang, S., Zhang, M., Hughes, C. E., Zhu, X., Dong, L., Ren, Z., & Chen, F. (2016). Factors controlling stable isotope composition of precipitation in arid conditions: An observation network in the Tianshan Mountains, Central Asia. *Tellus B: Chemical and Physical Meteorology*, *68*(1), 26206. https://doi.org/10.3402/tellusb.v68.26206

Wang, X., Carrapa, B., Sun, Y., Dettman, D. L., Chapman, J. B., Caves Rugenstein, J. K., Clementz, M. T., DeCelles, P. G., Wang, M., Chen, J., Quade, J., Wang, F., Li, Z., Oimuhammadzoda, I., Gadoev, M., Lohmann, G., Zhang, X., & Chen, F. (2020). The role of the westerlies and orography in Asian hydroclimate since the late Oligocene. *Geology*, *48*(7), 728–732. https://doi.org/10.1130/G47400.1

Wasiljeff, J., Salminen, J. M., Stenman, J., Zhang, Z., & Kaakinen, A. (2022). Oligocene moisture variations as evidenced by an aeolian dust sequence in Inner Mongolia, China. *Scientific Reports*, *12*(1), 1–14. https://doi.org/10.1038/s41598-022-09362-y

Wilcken, K. M., Codilean, A. T., Fülöp, R.-H., Kotevski, S., Rood, A. H., Rood, D. H., Seal, A. J., & Simon, K. (2021). Accelerator mass spectrometry of ^{10}Be and ^{26}Al at low nuclide concentrations. *Geochronology*, *4*(1), 339–352. https://doi.org/10.5194/gchron-2021-30

Wilcken, K. M., Fujioka, T., Fink, D., Fülöp, R.-H., Codilean, A. T., Simon, K., Mifsud, C., & Kotevski, S. (2019). SIRIUS performance: ^{10}Be, ^{26}Al and ^{36}Cl measurements at ANSTO. *Nuclear Instruments and Methods in Physics Research Section B: Beam Interactions with Materials and Atoms*, *455*, 300–304.

Windley, B. F., Alexeiev, D. V., Xiao, W., Kröner, A., & Badarch, G. (2007). Tectonic models for accretion of the central Asian Orogenic Belt. *Journal of the Geological Society, London*, *164*, 31–47. https://doi.org/10.1144/0016-76492006-022

Worden, R. H., Armitage, P. J., Butcher, A. R., Churchill, J. M., Csoma, A. E., Hollis, C., Lander, H., & Omma, J. E. (2018). Petroleum reservoir quality prediction: Overview and contrasting approaches from sandstone and carbonate communities. *Geological Society, London, Special Publications*, *435*(1), 1–31. https://doi.org/10.1144/SP435.21

Worden, R. H., & Burley, S. D. (2003). Sandstone diagenesis: The evolution of sand to stone. *Sandstone Diagenesis: Recent and Ancient*, *4*, 3–44. https://doi.org/10.1002/9781444304459.ch

Yang, W., Jolivet, M., Dupont-Nivet, G., & Guo, Z. (2014). Mesozoic–Cenozoic tectonic evolution of southwestern Tian Shan: Evidence from detrital zircon U/Pb and apatite fission track ages of the Ulugqat area, Northwest China. *Gondwana Research*, *26*(3–4), 986–1008. https://doi.org/10.1016/j.gr.2013.07.020

Zachos, J., Pagani, M., Sloan, L., Thomas, E., & Billups, K. (2001). Trends, rhythms, and aberrations in global climate 65 Ma to present. *Science*, *292*(5517), 686–693. https://doi.org/10.1126/science.1059412

Zech, R. (2012). A late Pleistocene glacial chronology from the Kitschi-Kurumdu Valley, Tien Shan (Kyrgyzstan), based on [10]Be surface exposure dating. *Quaternary Research*, *77*(2), 281–288. https://doi.org/10.1016/j.yqres.2011.11.008

Zhao, X., Zhang, H., Lv, H., Lü, Y., Li, X., Liu, K., Zhang, J., & Xiong, J. (2021). Signatures of tectonic-climatic interaction during the late Cenozoic orogenesis along the northern Chinese Tian Shan. *Basin Research*, *33*(1), 291–311. https://doi.org/10.1111/bre.12466

Zhuang, G., Hourigan, J. K., Koch, P. L., Ritts, B. D., & Kent-Corson, M. L. (2011). Isotopic constraints on intensified aridity in Central Asia around 12 Ma. *Earth and Planetary Science Letters*, *312*(1–2), 152–163. https://doi.org/10.1016/j.epsl.2011.10.005

Zubovich, A. V., Wang, X. Q., Scherba, Y. G., Schelochkov, G. G., Reilinger, R., Reigber, C., Mosienko, O. I., Molnar, P., Michajljow, W., Makarov, V. I., Li, J., Kuzikov, S. I., Herring, T. A., Hamburger, M. W., Hager, B. H., Dang, Y. M., Bragin, V. D., & Beisenbaev, R. T. (2010). GPS velocity field for the Tien Shan and surrounding regions. *Tectonics*, *29*(6), 1–23. https://doi.org/10.1029/2010TC002772

SUPPORTING INFORMATION

Additional supporting information can be found online in the Supporting Information section at the end of this article.